B.S.

NAVAL POSTGRADUATE SCHOOL
Monterey, California

THESIS

FRONTAL ANALYSIS AND ACOUSTIC PROPAGATION IN THE WESTERN ALBORAN SEA

by

Richard Peerson Adams

December 1977

Thesis Advisors: R. H. Bourke
A. B. Chace

Approved for public release; distribution unlimited.

UNCLASSIFIED

SECURITY CLASSIFICATION OF THIS PAGE (When Data Entered)

REPORT DOCUMENTATION PAGE	READ INSTRUCTIONS BEFORE COMPLETING FORM
1. REPORT NUMBER / 2. GOVT ACCESSION NO.	3. RECIPIENT'S CATALOG NUMBER
4. TITLE (and Subtitle): Frontal Analysis and Acoustic Propagation in the Western Alboran Sea	5. TYPE OF REPORT & PERIOD COVERED: Master's Thesis; December 1977
	6. PERFORMING ORG. REPORT NUMBER
7. AUTHOR(s): Richard Peerson Adams	8. CONTRACT OR GRANT NUMBER(s)
9. PERFORMING ORGANIZATION NAME AND ADDRESS: Naval Postgraduate School, Monterey, California 93940	10. PROGRAM ELEMENT, PROJECT, TASK AREA & WORK UNIT NUMBERS
11. CONTROLLING OFFICE NAME AND ADDRESS: Naval Postgraduate School, Monterey, California 93940	12. REPORT DATE: Dec 1977; 13. NUMBER OF PAGES: 85
14. MONITORING AGENCY NAME & ADDRESS(if different from Controlling Office): Naval Postgraduate School, Monterey, California 93940	15. SECURITY CLASS. (of this report): Unclassified; 15a. DECLASSIFICATION/DOWNGRADING SCHEDULE

16. DISTRIBUTION STATEMENT (of this Report)

Approved for public release; distribution unlimited.

17. DISTRIBUTION STATEMENT (of the abstract entered in Block 20, if different from Report)

18. SUPPLEMENTARY NOTES

19. KEY WORDS (Continue on reverse side if necessary and identify by block number)

20. ABSTRACT (Continue on reverse side if necessary and identify by block number)

Oceanic frontal activity in the western Alboran Sea of the Mediterranean Sea was investigated to evaluate spatial and temporal variability. Subsurface features were compared with DMSP sensed sea surface temperature to estimate the feasibility of determining frontal location from DMSP photography. Low frequency sound propagation across the

DD FORM 1 JAN 73 1473 (Page 1) EDITION OF 1 NOV 65 IS OBSOLETE S/N 0102-014-6601

UNCLASSIFIED

SECURITY CLASSIFICATION OF THIS PAGE (When Data Entered)

251 450

(cont)

front was modeled to evaluate the effect of the frontal system on propagation loss.

Approved for public release; distribution unlimited

Frontal Analysis and Acoustic Propagation in the Western Alboran Sea

by

Richard Peerson Adams
Lieutenant Commander, United States Navy
B.S., University of Virginia, 1965

Submitted in partial fulfillment of the requirements for the degree of

MASTER OF SCIENCE IN SYSTEMS TECHNOLOGY

from the

NAVAL POSTGRADUATE SCHOOL

December 1977

Author: Richard P Adams

Approved by: Robert H Bourke
Thesis Advisor

Allen B Chaney
Thesis Advisor

W L Hurt
Chairman, ASW Group

Jack R Borsting
Academic Dean

ABSTRACT

Oceanic frontal activity in the western Alboran Sea of the Mediterranean Sea was investigated to evaluate spatial and temporal variability. Subsurface features were compared with DMSP sensed sea surface temperature to estimate the feasibility of determining frontal location from DMSP photography. Low frequency sound propagation across the front was modeled to evaluate the effect of the frontal system on propagation loss.

TABLE OF CONTENTS

LIST OF FIGURES

ACKNOWLEDGEMENT

The author wishes to thank Dr. R. H. Bourke and LCDR A. B. Chace for their assistance in the preparation of this thesis, and my wife Cam for her encouragement and patience.

I. INTRODUCTION

A. OVERVIEW

Anti-submarine warfare (ASW) patrol aircrews operating in the western Alboran basin of the Mediterranean Sea have frequently noted that the acoustic environment is highly variable and difficult to predict. They have commented that acoustic predictions often seem to poorly represent the encountered propagation and contribute little toward mission planning. These practical considerations and the continued importance of the Gibraltar Strait and its approaches to the U.S. Sixth Fleet suggest that there is a need for detailed investigation of the nature of acoustic propagation in the western Alboran Sea.

B. BACKGROUND AND GENERAL OCEANOGRAPHY

In July and August 1962 a comprehensive oceanographic study of the Alboran Sea was conducted by French scientists and reported by Lanoix (1974). He described the basin immediately east of Gibraltar, shown in Figure 1, as a narrow channel in which Atlantic Ocean water with salinity of approximately 36.3‰ and temperatures between 15°C and 24°C flows eastward in the upper 100 m. The Atlantic water overlies westward moving Mediterranean water located at depths greater than 300 m and identified by temperatures between 12.7°C and 15°C with salinity near 38.4‰. Between these two regimes, from about 100 m to 300 m depth, is a transition layer

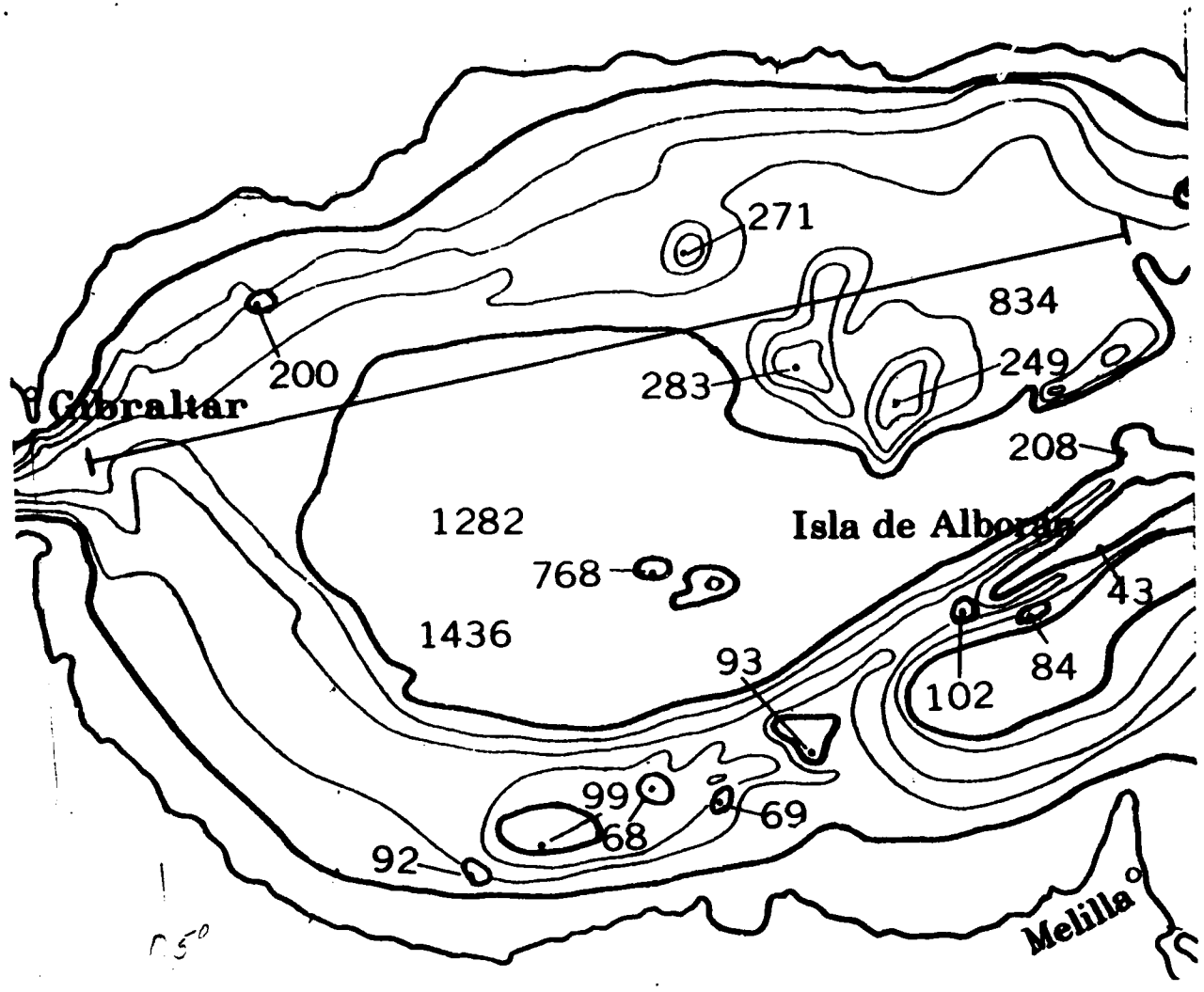

Figure 1. Western Alboran basin of the Mediterranean Sea. Temperature section line shown. Bathymetry in meters.

characterized by a steep salinity gradient of about 2‰ in 100 m. The investigation established that in the Alboran Sea significant temperature changes occur over short vertical and horizontal distances. As illustrated by Figure 2, temperatures along the track shown in Figure 1 at a depth of 100 m vary as much as 5°C over distances of approximately 50 km. This horizontal temperature variation produces sound speed changes of as much as 25 meters/sec, thereby causing significant refraction of the acoustic wave front and consequent acoustic intensity modification.

The salinity structure reported by the Lanoix study is illustrated in Figure 3, which shows a salinity section along 4° - 15'W longitude. The horizontal salinity gradients evident in Figure 3 at 100 m depth produce a variation in sound speed of less than 2.5 m/sec over 50 km. Since the temperature section in Figure 2 shows temperature gradients equating to approximately 25 m/sec over similar ranges, horizontal salinity gradients do not significantly alter acoustic propagation.

Circulation patterns change sound propagation principally by modifying the spatial distributions of temperature, salinity, suspended scattering material and biological activity. Although the separate measurement of these parameters provides an estimate of their individual effect on acoustic propagation, the Alboran Sea surface currents shown in Figure 4 are most useful as an aid in evaluating the boundaries where significant changes in sound transmission occur.

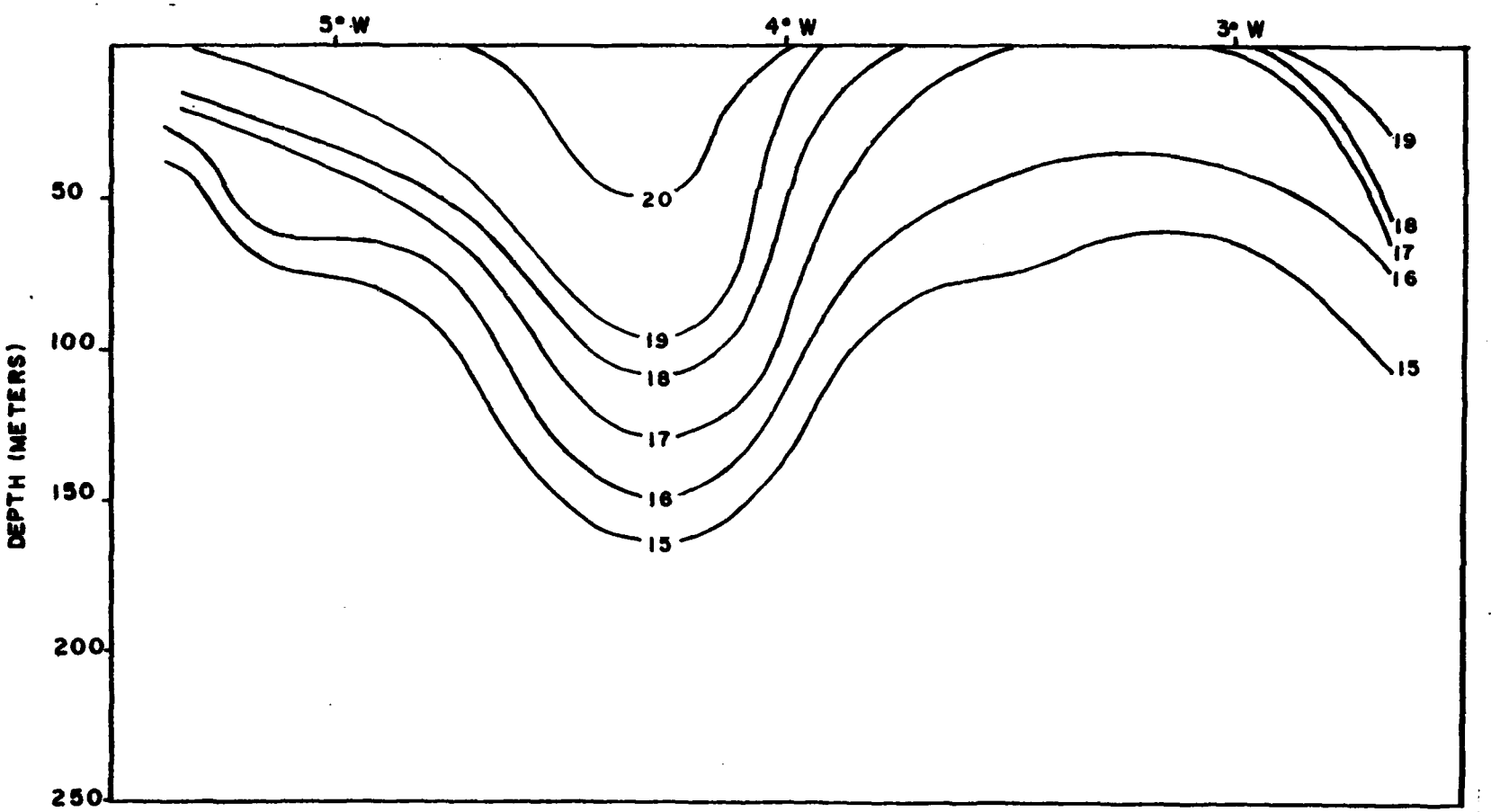

Figure 2. Temperature cross-section of the western Alboran Sea, west to east, October 1976. Section line shown in Figure 1. Isotherms in °C. (after Mommsen, 1976)

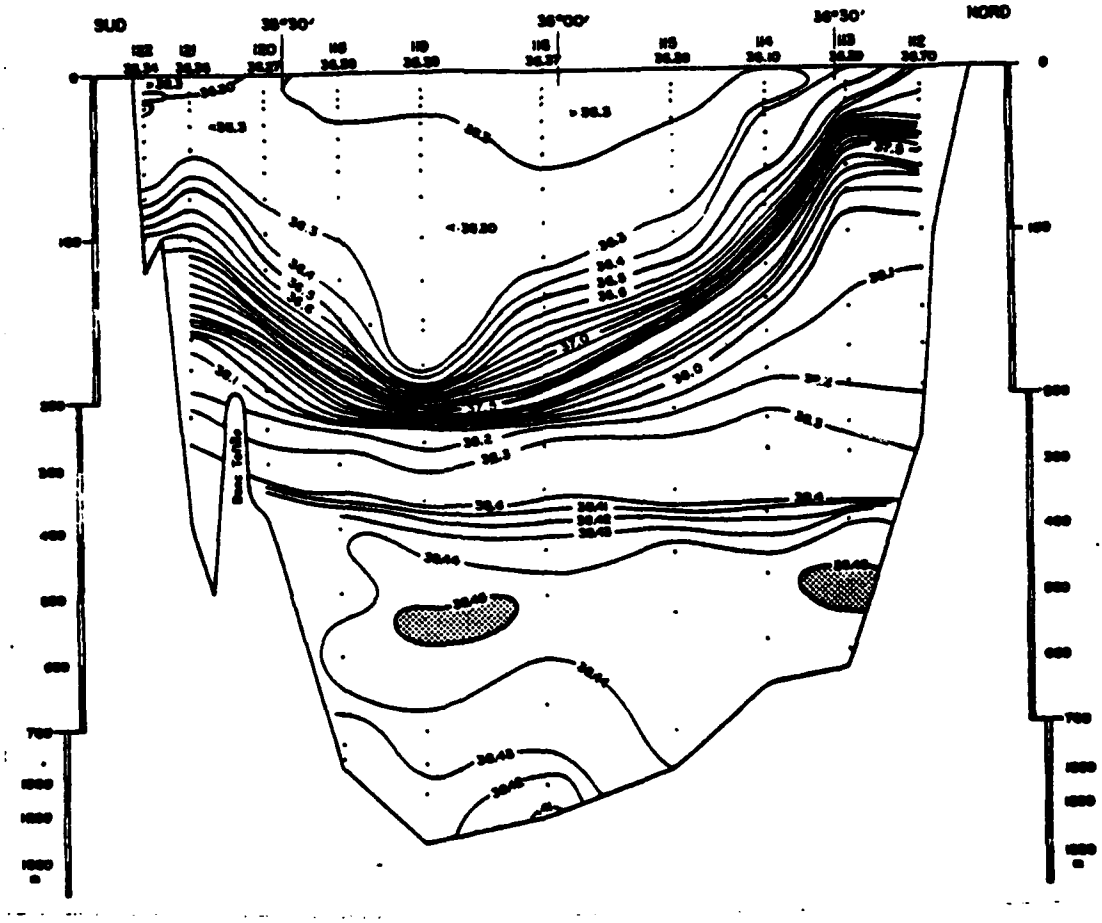

Figure 3. Salinity cross-section, south to north across the Alboran Sea at 4°W (‰). July-August 1962. Depth in meters. (after Lanoix, 1974)

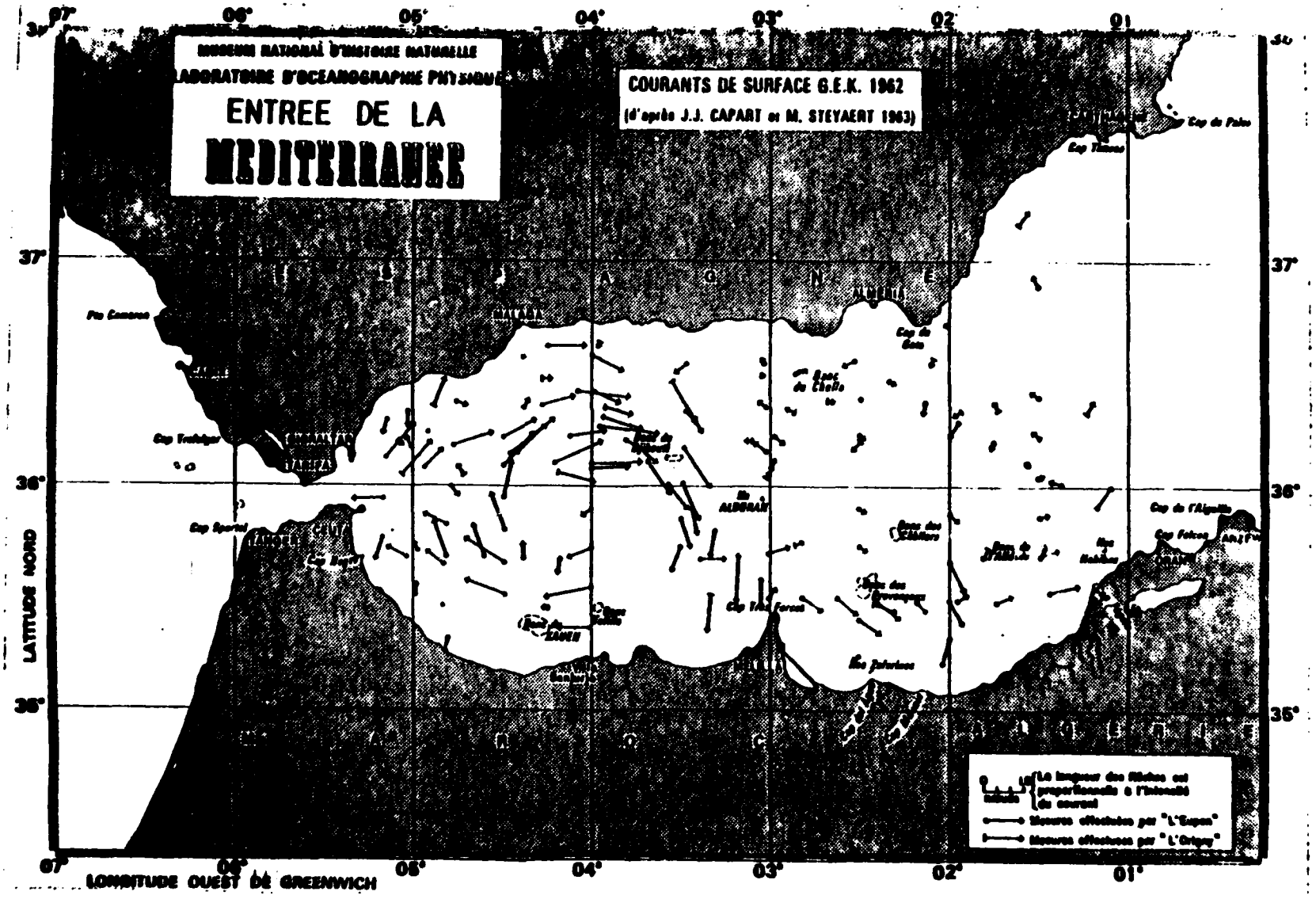

Figure 4. Surface currents of the western Alboran Sea, July-August 1962. (Lanoix, 1974)

Figures 2, 3 and 4 together clearly illustrate the predominate oceanographic and acoustic feature of the western Alboran Sea: a circulation pattern of shallow Atlantic water entering the Mediterranean Sea and forming an anti-cyclonic gyre centered at about 35°-50'N, 4°-10'W over the western Alboran basin, and extending to 200 m depth with a strong horizontal temperature gradient, or front, around its periphery.

Oceanographic investigations of the Alboran Sea conducted after the 1962 French study confirmed the thermal features Lanoix described. Surface and subsurface temperature observations obtained in July, September, October and November 1976 and reported by Mommsen (1976) agree with the oceanographic structure shown by Lanoix. Mommsen found that thermal gradients of about 5°C in 50 km (30 nm) were present to depths of 200 m and that these gradients represented the edges of the western Alboran gyre. Cheney (1977, p. 2) made use of April-May 1976 aircraft dropped bathythermographs (AXBT) to describe acoustic frontal zones in the western Mediterranean. He suggested that an acoustic front be defined as "... a coherent, recognizable boundary separating different acoustic regimes as characterized by SLD [Sonic Layer Depth, the depth of the first sound speed maximum below the surface] and SCD [Sound Channel Depth, the depth of minimum sound speed]." Further, he required that either SCD or SLD, or both, change by more than 50 m within 25-35 km. The study reported by Cheney showed that in the Alboran Sea significant SLD and SCD changes

do occur over horizontal distances short enough to qualify as acoustic fronts. In the western Alboran basin, frontal zones were found to coincide with the northern edge of the anti-cyclonic gyre. Cheney also found that the western Alboran Sea could be divided into two distinct acoustic regimes, separated by the acoustic front. North of the acoustic front conditions were defined by a relatively shallow SLD and SCD at about 40 m and 140 m, respectively. To the south, where warm Atlantic surface water is trapped in the gyre, the SLD is approximately 160 m and SCD near 220 m.

The bathymetry of the western Alboran basin is shown in Figure 1. The shape of the basin is dominated by the shallow Gibraltar Strait sill in the west, and the Alboran Island rise in the east. It is important to note that the generally bathtub-like appearance is altered by shallower depths to the north and a steeper upslope on the south. The Lanoix study indicated that these bathymetric features and geostrophic flow play a large role in producing a geographically stable gyre. The study also demonstrated that the gyre induces a converging Ekman transport with a subsidence of warm Atlantic surface water at its center and a compensating upwelling of colder Mediterranean water at the gyre edges, especially to the north.

The upwelling of cooler Mediterranean water along the edges of the western Alboran gyre can create sea surface temperature (SST) gradients which are detectable by satellite infrared (IR) photography. This imagery may then be used to

define the circulation pattern, and of particular acoustic significance, the location of subsurface thermal gradients. Recent comparisons of Defense Meteorological Satellite Program (DMSP) photography of the Alboran SST and concurrent sampling of the vertical thermal structure have demonstrated that remotely sensed surface temperature gradients can reflect the location of the sub-surface features of the western Alboran front (Cheney, 1977; Mommsen, 1976; Stephenson, 1977). Eubanks, Gallagar and Browning (1977) have noted that this agreement between SST and subsurface features is especially apparent in summer when relatively little mixing of the upper layers occurs. It is less observable in winter when colder surface water and a deeper mixed layer obscure upwelling at the gyre perimeter.

Few winter oceanographic studies of the western Alboran Sea are reported in the literature. However, analysis of January 1977 bathythermograph (BT) and AXBT data by the National Oceanographic Office (1977) shows SCD gradients which correspond in intensity and location to the acoustic front found in summer at the gyre's northern edge. These subsurface temperature observations support Lanoix's suggestion that the gyre is a permanent oceanographic feature of the western Alboran Sea.

C. ACOUSTIC EFFECTS

In recent years the effect of an oceanic thermal front on acoustic propagation has been an area of intense investigation (Eubanks et al., 1977; Gemmil and Khedouri, 1974; Khedouri and

Gaborski, 1977; Levenson and Doblar, 1975; Schully-Powers et al., 1975; Vastano and Owens, 1973). These investigations have established that thermal gradients of the strength found in the western Alboran Sea cause significant changes in acoustic propagation. Modifications in convergence zone spacing, focusing, and limiting depths have been observed. Changes in the depth and intensity of sound trapped in surface ducts and deep sound channels have also been noted (Levenson and Doblar, 1975; Schully-Powers et al., 1975).

The acoustic effects of an oceanic front in the western Alboran Sea is of special significance to ASW operations in the western Mediterranean Sea. Current U.S. Navy acoustic predictions assume a homogeneous water mass, constant bottom depth, and uniform bottom loss (Director of Naval Oceanography and Meteorology, 1976). These assumptions are appropriate for most areas of the open ocean where relatively homogeneous conditions prevail over acoustic ranges of interest. However, such assumptions in the distinctly non-homogeneous western Alboran basin will certainly limit the accuracy of acoustic predictions.

D. OBJECTIVES

It is the purpose of this thesis to provide a good estimate of the geographical variability of the western Alboran acoustic front. The position of the front is determined for both winter and summer for several years. Comparisons are made between DMSP SST photography and the oceanographic features of the Alboran Sea to assess the possibility of determining frontal position from remotely sensed SST imagery.

Acoustic raytracing techniques are employed to provide an indication of sound transmission paths and propagation losses within the northern and southern acoustic regimes and across the acoustic front.

II. TREATMENT OF DATA

A. SOURCES

Bathythermograph and Nansen cast data for the area 3°W to 5°W and 35°N to 37°N were obtained for several years between 1948 and 1973 from the Fleet Numerical Weather Central (FNWC) Hydroclimatological Data Retrieval Program (Lewitt et al., 1977). Additional data for the years 1973-1977 were obtained from the XBT and AXBT files of FNWC, the August-September 1975 cruise of the USNS KANE, and unpublished January 1977 data from the Naval Oceanographic Office.

Defense Meteorological Satellite Program (DMSP) infrared photographs of the Alboran Sea were obtained from Fleet Weather Central (FWC), Rota, Spain. The photographs provided sea surface temperature gradients and showed good coverage of the western Alboran Sea in winter, summer and transition months.

B. METHODOLOGY

Mediterranean Sea oceanographic seasons can be divided into two distinct periods, summer and winter, in which physical water properties are quasi-stationary. The oceanographic seasons between, spring and fall, are characterized by gradual transitions in water properties (Colborn, 1975; Russell, 1975). Comparisons drawn between winter and summer conditions thus clearly illustrate the limits of seasonal variability and were used to indicate the effect of seasonal changes on frontal

location, acoustic propagation, and sea surface temperature. August and September were selected as the months providing most typical summer conditions and January-March as the period typifying winter. The oceanographic and acoustic characteristics of each season will be discussed in the next sections.

Temperature, salinity and density gradients are commonly used to define oceanic fronts. Although the acoustic effect of these parameters, when considered singly, is readily understood, their collective effects are less easily evaluated. Sound speed profiles were used to eliminate much of this difficulty and permit almost direct visualization of the impact of spatially changing oceanographic parameters on sound transmission.

The Integrated Carrier ASW Prediction System (ICAPS) was used to calculate sound speed profiles from the BT data. ICAPS was also used to extrapolate profiles to maximum water depth using climatological salinity and deep temperature values. The sound speed profiles were then used to plot maps of sonic layer depth and sound channel axis depth. The plots were interpreted using the acoustic front definition suggested by Cheney, i.e., at least 50 m change in SCD or SLD, or both, over a 25-35 km distance.

The position of the front in winter and summer was constructed for each year for which sufficient data were available. Mapping the front in this manner provided an indication of the spatial and temporal variability of frontal position and strength.

DMSP infrared photographs of sea surface temperature were then compared with appropriate frontal positions. This comparison was used to develop an estimate of the feasibility of locating the frontal zone from remotely sensed data in all seasons.

Sound transmission in the Alboran Sea was modeled for three omni-directional acoustic sources at 100 m depth, assumed positioned as follows:

Position 1 -- 36°-07'N 3°-28'W

Position 2 -- 36°-05'N 4°-12'W

Position 3 -- 36°-02'N 4°-44'W

These positions are shown on each of the maps of SLD and SCD in Figures 5-15.

Sound propagation paths were oriented approximately north, south and west from Position 1, north and south from Position 2, and north, south and east from Position 3. Sound speeds along each propagation path were taken from a year with data density sufficient to clearly show typical frontal features. The FNWC JCRAYB raytracing program (FNWC, 1977) was used to provide a visual estimate of acoustic propagation along each path and transmission loss was calculated using the RP-70 ray acoustic program. Frequencies of 50, 300 and 1800 Hz were used. Bathymetry was digitized at 200 m depth intervals and bottom loss values were estimated from the bottom composition using five bottom loss categories. Shallow areas were assigned a high bottom loss value of 4 while areas of the Alboran basin deeper than 500 m were assumed to have a moderate bottom loss value of 3.

Sound speed sections were drawn along each propagation path and combined with plots of sonic layer and sound channel depth. This format makes significant changes in SLD and SCD readily apparent and provides direct spatial comparison between gradients in SLD or SCD and sound propagation changes. The plots of sound isotachs allow rapid estimation of sound channel and layer strength, dimensions, and focusing ability, as well as depict oceanographic features associated with the Alboran circulation.

III. RESULTS

A. FRONTAL VARIABILITY

The approximate location of the western Alboran Sea acoustic front in summer for various years is shown in Figures 5 through 9. Each figure is a map of sound channel depth for the year indicated. Shown in cross-hatch are the zones in which the SCD changes by at least 50 m in 25-35 km (14-19 nm). Sonic layer depth for these years is not shown, since in summer the Alboran Sea SLD is usually less than 25 m and the small changes found are not acoustically significant.

Frontal geographic stability is evident in these figures. Between the Strait of Gibraltar and 4°W the front is close to and roughly parallels 36°N. In this area channel depth shoals from about 200 m south of the 36°N parallel to approximately 150 m north of 36°N, over a distance of less than 30 nm. From 4°W to 5°W the frontal zone location appears more variable, but is generally oriented southeast from 36°N, 4°W. The frontal zones shown in Figures 5-9 agree reasonably well with the location of the northern edge of the anti-cyclonic gyre described by Lanoix and illustrated by Figures 2, 3 and 4.

An additional acoustic frontal zone appears along the southern Spanish coast in Figures 5 and 6 corresponding to the bathymetrically induced upwelling of deep Mediterranean water. Because this acoustic front is located within 10 nm of the southern Spanish coast, it is not considered important for ASW operations.

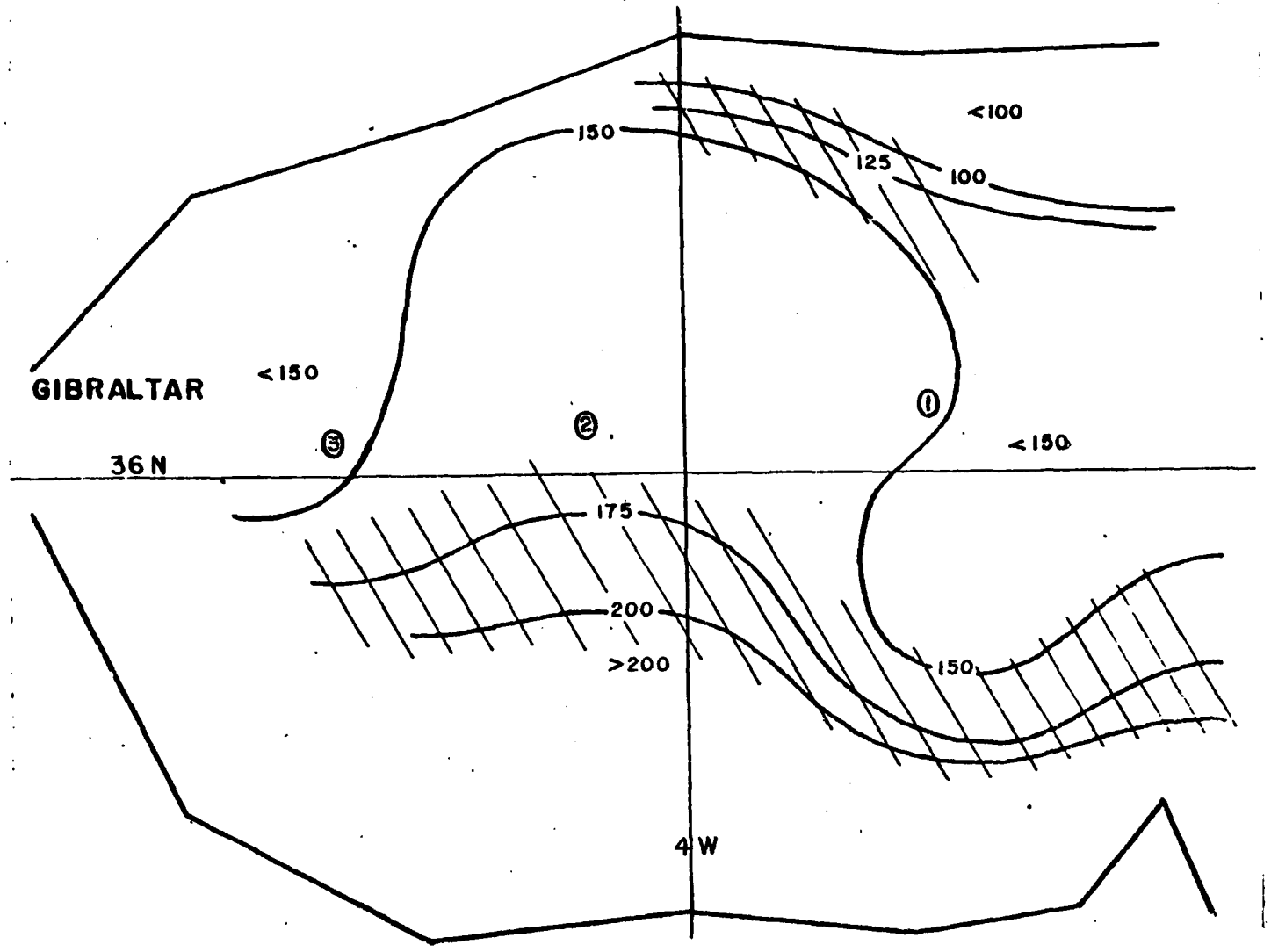

Figure 5. Sound channel depth, summer 1957 (contours in meters)

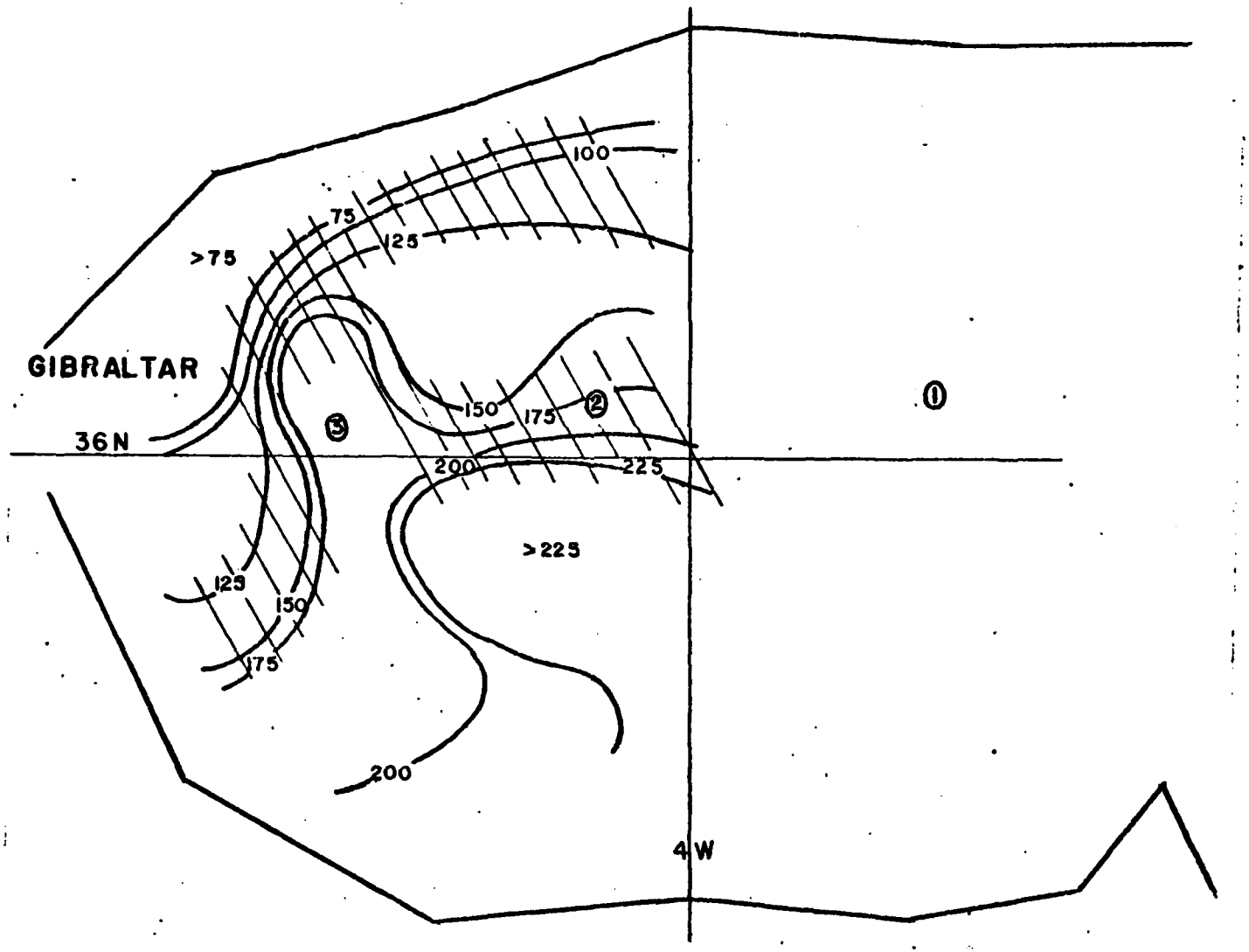

Figure 6. Sound channel depth, summer 1962 (contours in meters)

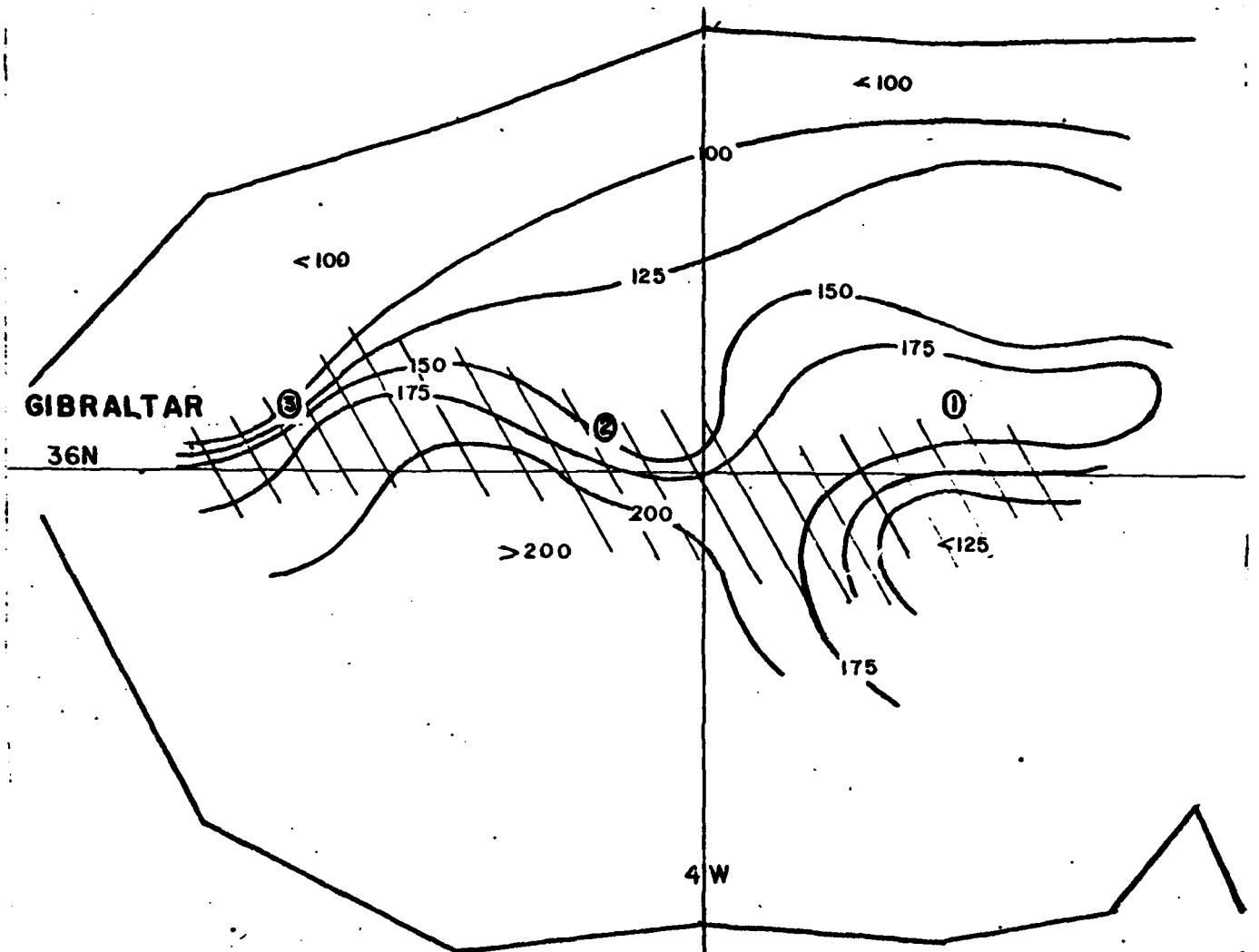

Figure 7. Sound channel depth, summer 1969 (contours in meters)

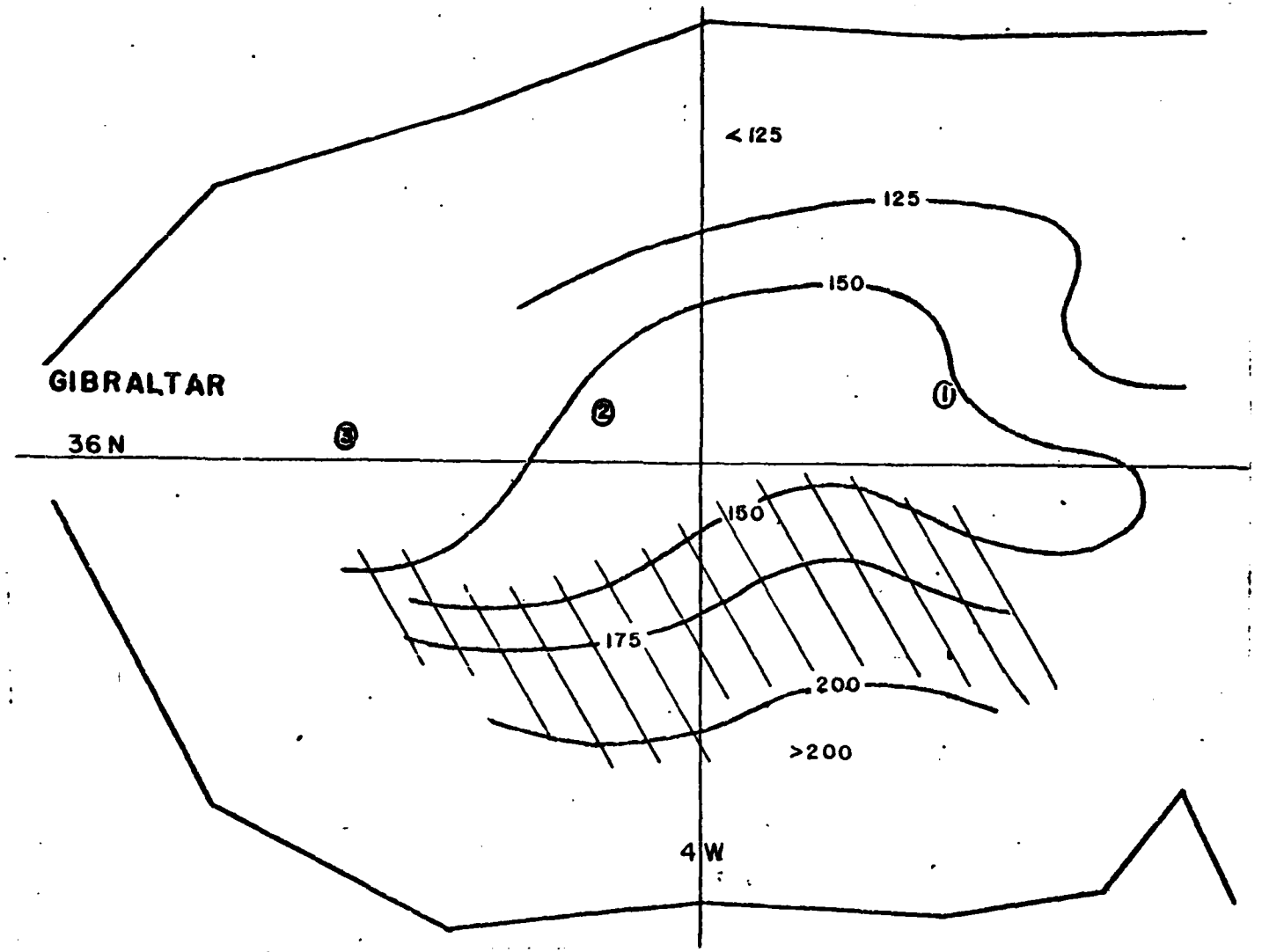

Figure 8. Sound channel depth, summer 1970 (contours in maters)

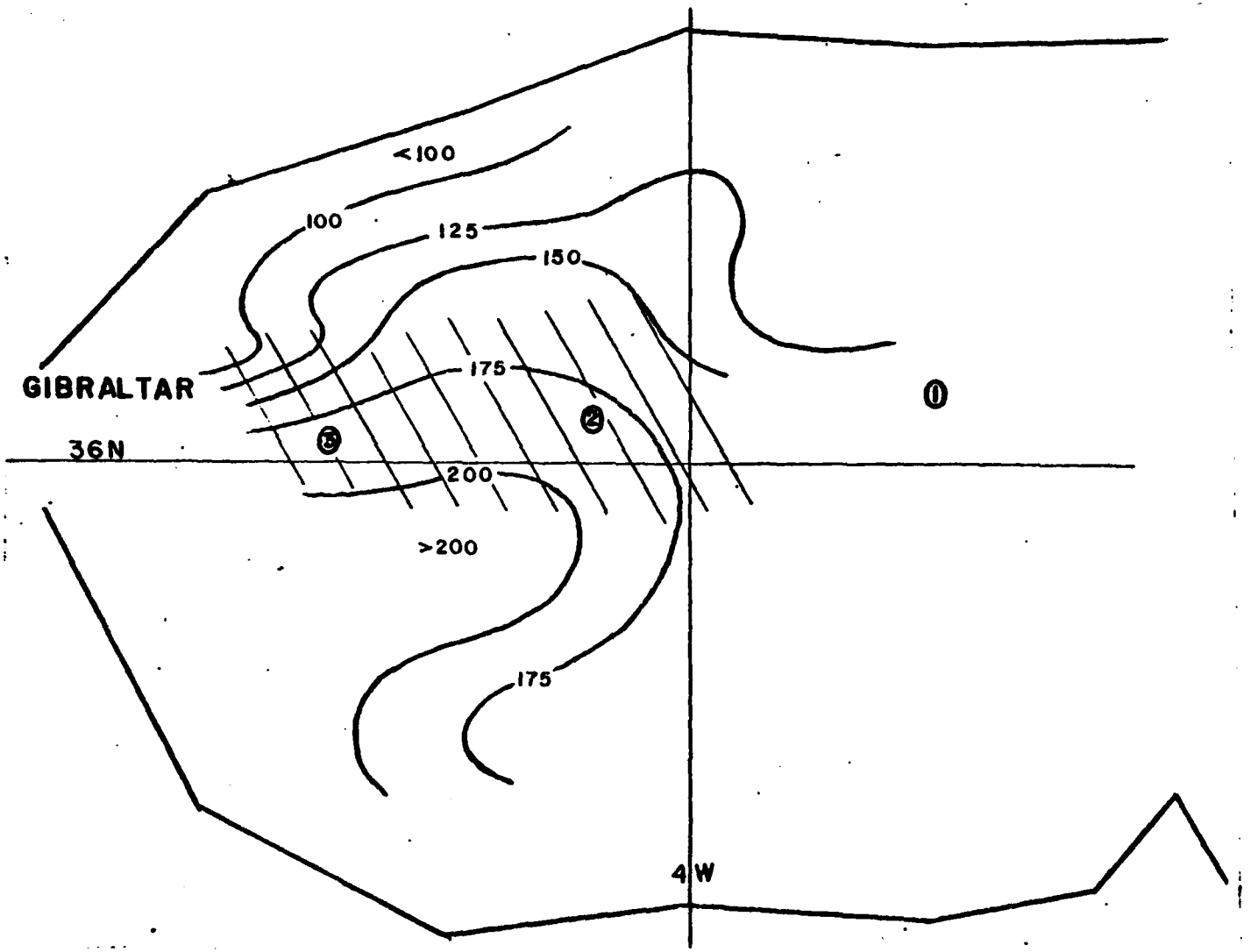

Figure 9. Sound channel depth, summer 1975 (contours in meters)

The year-to-year variation in the SCD gradient of the Alboran front is illustrated by comparing Figures 5 and 6. Figure 5 shows an SCD gradient at 4°W of about 1.3 m/km (2.4 m/nm) in 1957, while the gradient shown in Figure 6 at 4°30'W is near 4.0 m/km (7.5 m/nm) for 1962. These gradient differences are induced by variations in the horizontal distances over which the sound channel depth changes. It is thought that the variability in frontal zone width is caused by the changing volume flow rates of Atlantic Ocean water entering the Strait of Gibraltar and the resulting changes in water mass properties.

The estimated position of the Alboran front in winter is shown in Figures 10 through 15. Figures 10 and 11 are plots of sound channel depth and sonic layer depth for January 1948 and Figures 12 and 13 are plots of SCD for January 1971 and 1975, respectively. Layer depth plots for these latter years are not shown since the SLD gradients found were too weak to be of acoustic significance. Figures 14 and 15 show SCD and SLD gradients for January 1977.

The winter position of the western Alboran acoustic front appears to be somewhat more variable than that in summer. However, the general features noted in summer persist, especially the division of the basin at about 36°N into two acoustic regimes. To the north is a region where the sound channel is shallow with depths of about 100 m, while to the south the SCD is generally greater than 200 m. East of 4°W the front does not appear to follow the perimeter of the

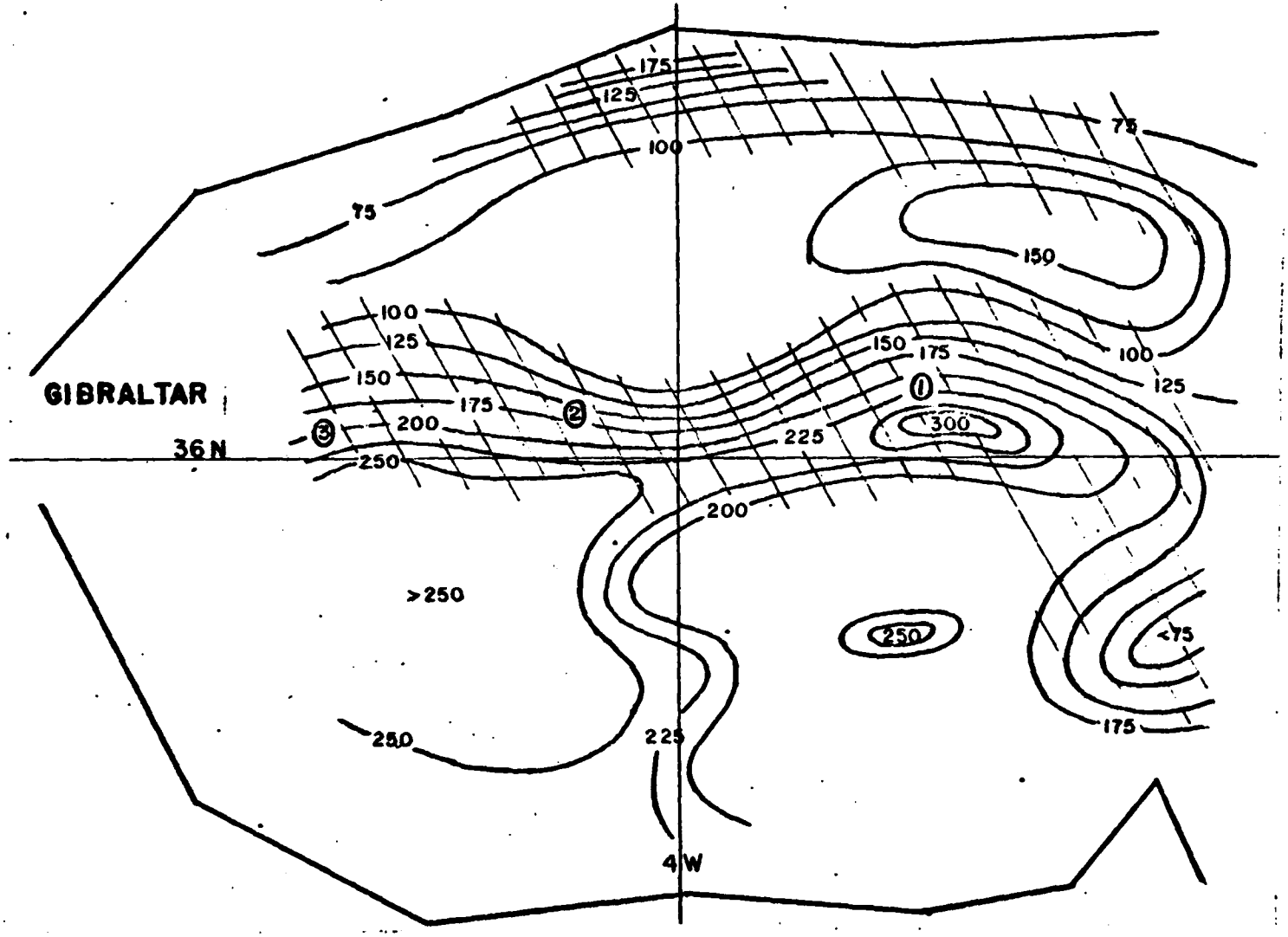

Figure 10. Sound channel depth, winter 1948 (contours in meters)

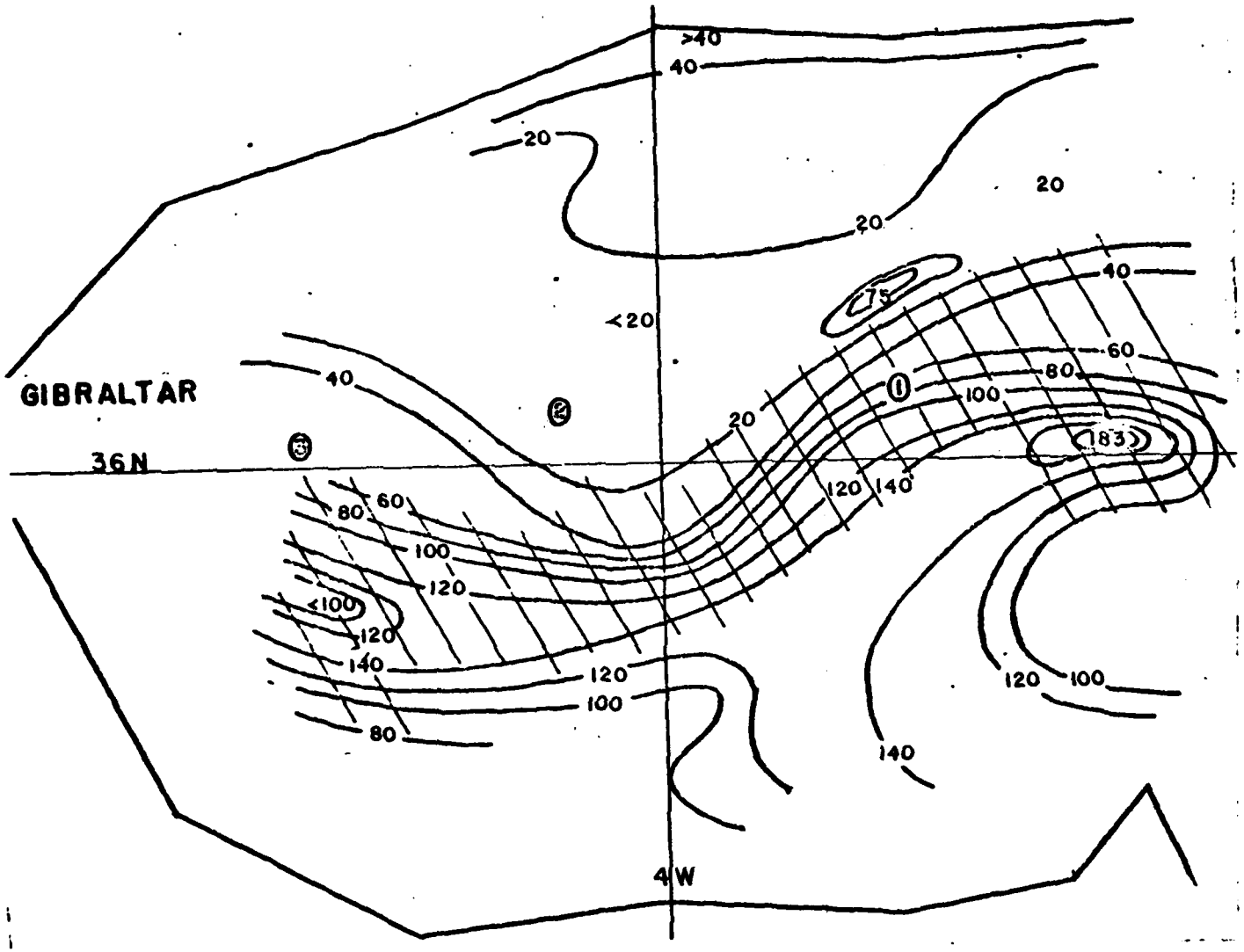

Figure 11. Sonic layer depth, winter 1948 (contours in meters)

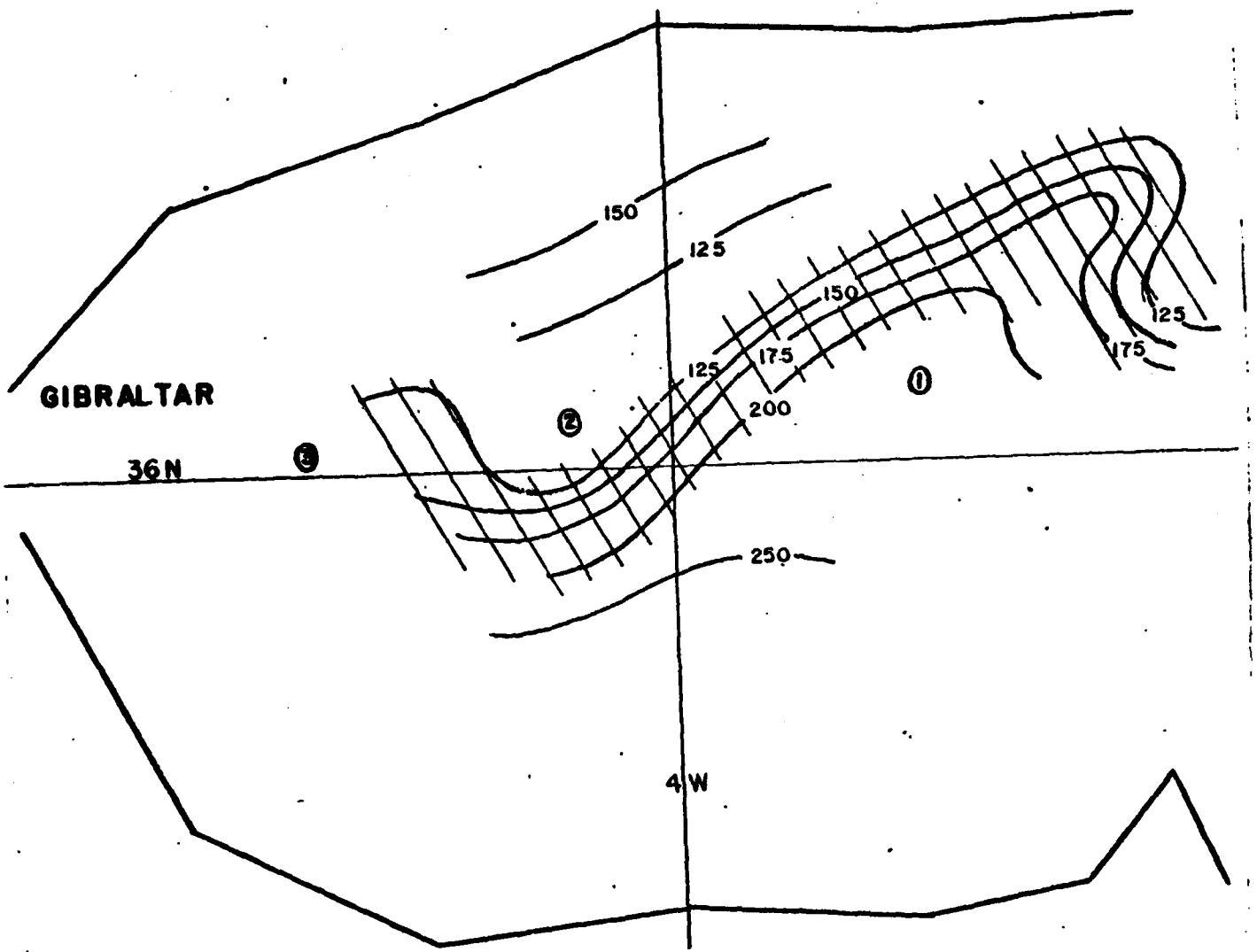

Figure 12. Sound channel depth, winter 1971 (contours in meters)

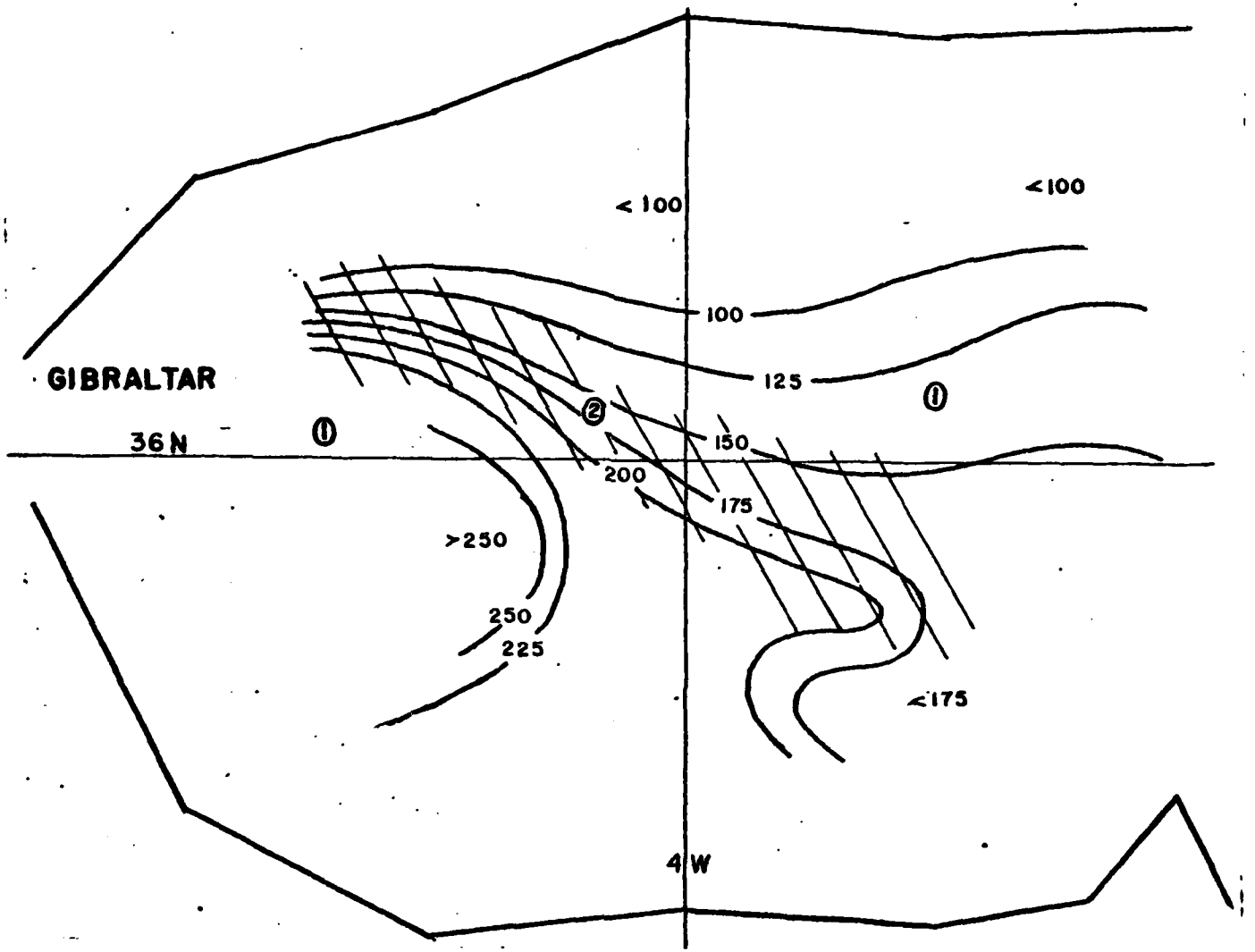

Figure 13. Sound channel depth, winter 1975 (contours in meters)

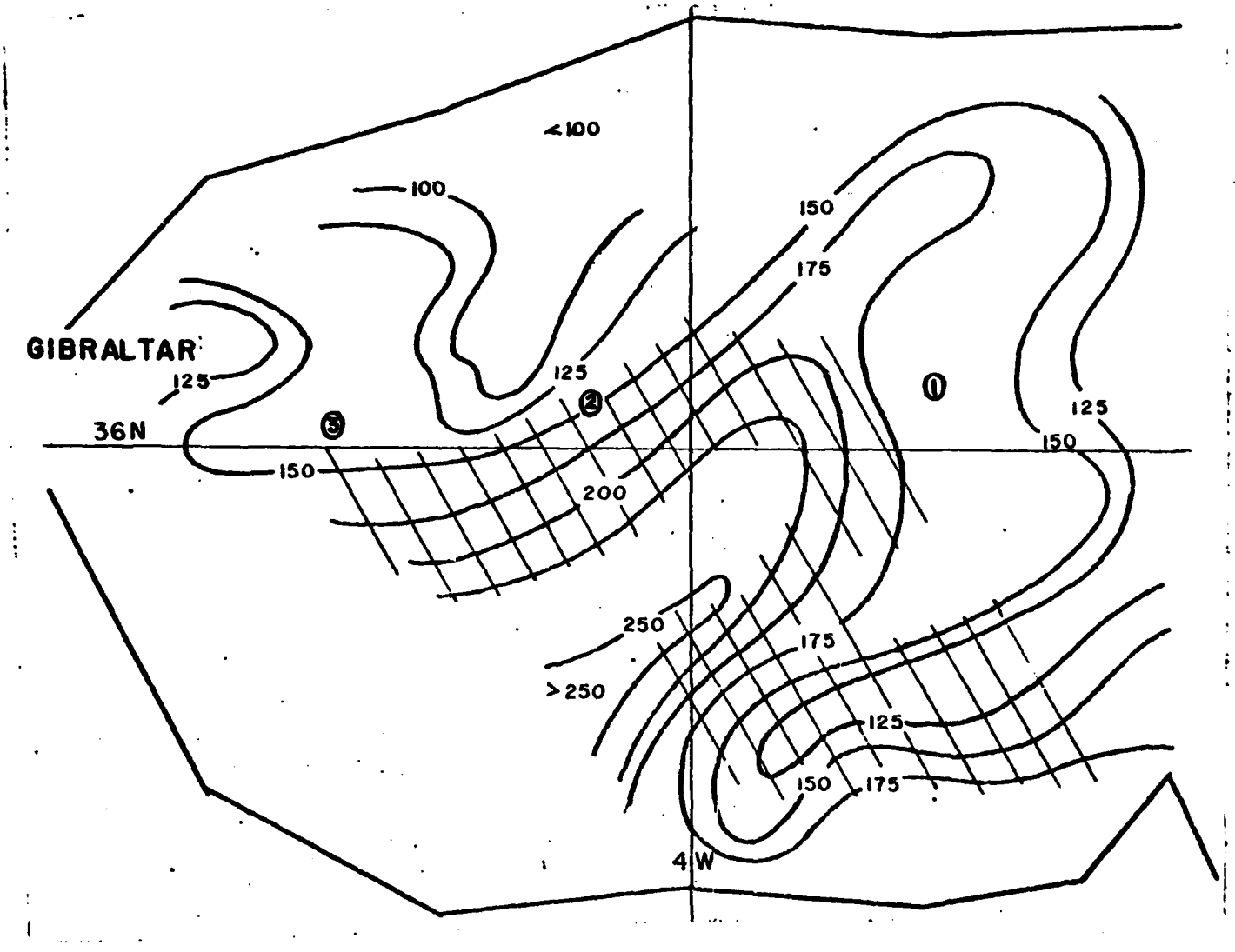

Figure 14. Sound channel depth, winter 1977 (contours in meters)

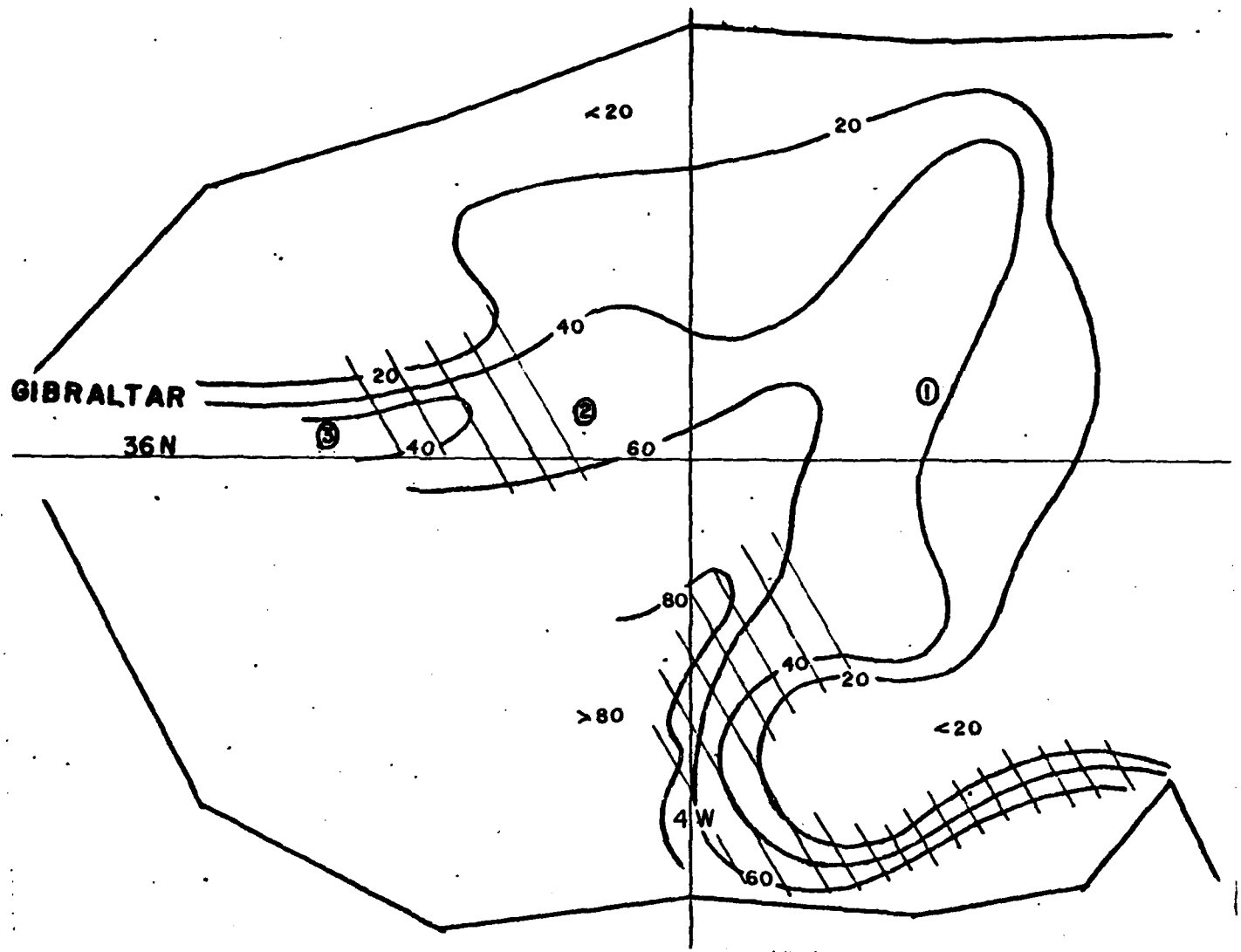

Figure 15. Sonic layer depth, winter 1977 (contours in meters)

anti-cyclonic circulation of Atlantic surface water, but becomes increasingly variable with the direction of the front apparently less influenced by geostrophic flow and bathymetry.

The winter frontal position indicated in Figure 10 is estimated from the SCD gradients, while Figure 11 shows the front based on SLD changes. Figures 14 and 15 present similar data for January 1977. The frontal position derived from the SLD map shown in Figure 11 closely coincides with acoustically significant sound channel depth gradients. However, the absence of significant SLD gradients in January 1971 and 1975 and the small layer depth changes shown in Figure 15 suggest that SLD may not be a reliable indicator of frontal position. Figure 15 also shows that layer depth gradients may be horizontally offset from the SCD defined frontal position (Figure 14) for significant distances.

The frontal zone adjacent to the Spanish coast appearing in Figure 10 suggests that the upwelling of deep Mediterranean water noted in the summer may continue during the winter season. The proximity of this front to the Spanish coast limits its ASW significance.

The strength of the SCD gradients shown in Figures 10, 12, 13 and 14 vary from approximately 3.6 m/km (6.7 m/nm) in Figure 10 to about 1.3 m/km (2.4 m/nm) found in Figure 14. This gradient range is nearly identical with the range of frontal strength found in summer.

The year-round geographic stability of the western Alboran front is of considerable potential usefulness for improving

the prediction of sound propagation in the eastern Gibraltar approaches. Although frontal position variability increases east of 4°W longitude, Figures 5 through 15 support the division of the western Alboran basin into north and south acoustic regimes. The sound channel and layer depth plots also suggest that the frontal position is largely seasonally independent, with the northern sector identified by relatively shallow SCD and SLD and the southern area characterized by deeper channel and layer depths.

As previously noted, the western Alboran circulation is largely responsible for creating both an upwelling-associated surface temperature gradient and an almost seasonally independent subsurface front. The observed relationship of these oceanographic features makes it reasonable to expect that whenever strong SST gradients are present they will coincide with sub-surface frontal features.

B. SATELLITE OBSERVATIONS

DMSP infrared imagery of the western Alboran in summer is shown in Figure 16. This photograph shows a sea surface temperature pattern that outlines the anti-cyclonic circulation in the western basin. Although Mommsen (1976) and Stephenson (1977) noted that clouds or low layers of moist air can be misinterpreted as cold water, they demonstrated that remotely sensed sea surface temperatures agree well with measured temperatures and can be considered equivalent to numerous, surface observations. Mommsen and Stephenson showed that DMSP sensed summer sea surface temperature gradients reflect

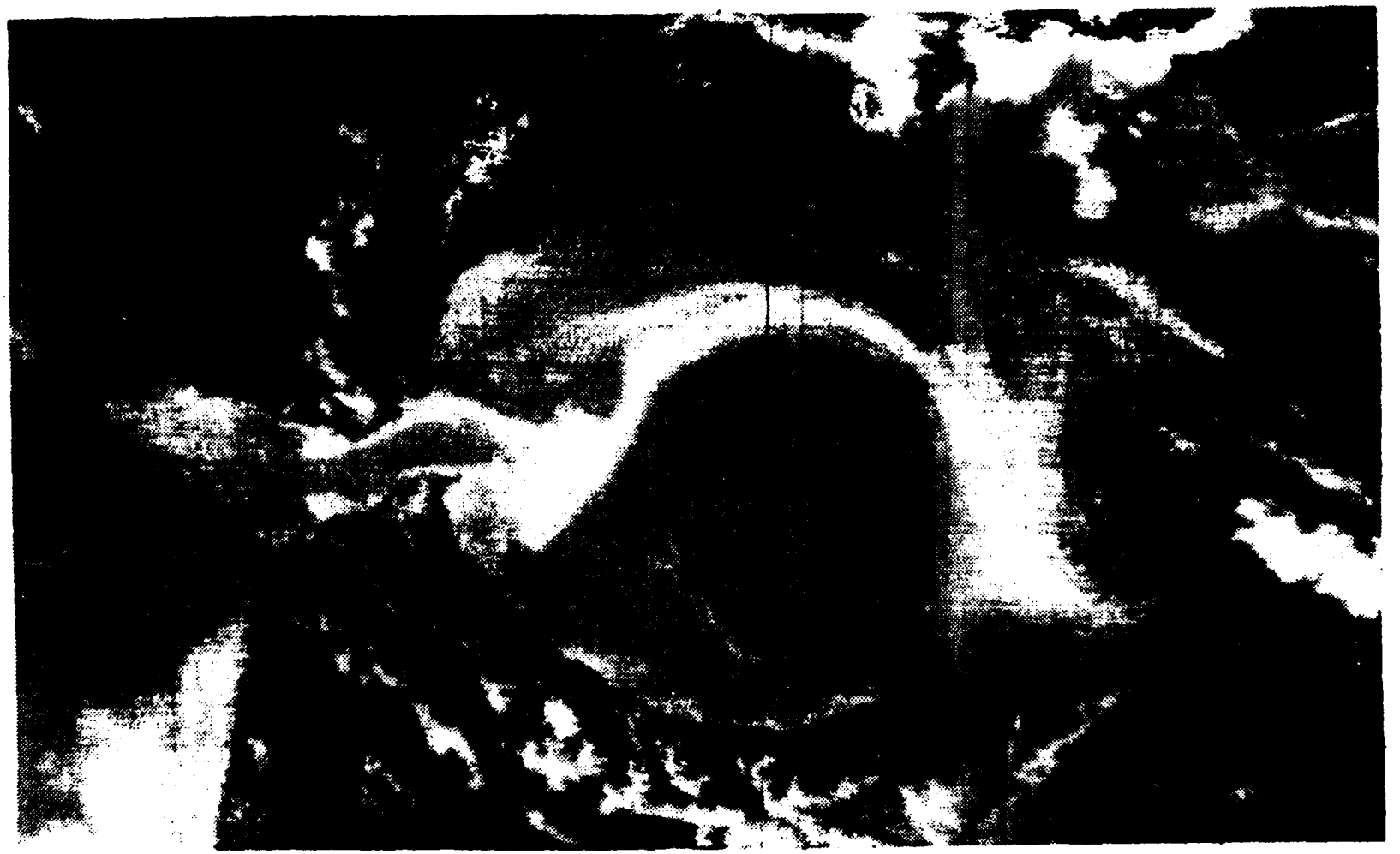

Figure 16. DMSP infrared photograph of the western Alboran Sea, summer 1977. Lighter shading indicates cooler sea surface temperatures.

the location of subsurface temperature changes; Cheney (1977) found that these gradients correspond to an acoustic front. These observations, coupled with the close agreement between the front location depicted in Figures 5-9, and the position of SST gradients shown in Figure 16, suggest that DMSP IR photography can be used to locate the summer Alboran front.

The ability of remotely sensed SST to show the Alboran front is obviously limited by the strength of the surface temperature gradients. Figure 17 shows the Alboran Sea in early fall when temperature gradients appear significantly less intense. The figure indicates the effect of changing wind patterns and lower wind stresses which produce diminished water mass convergence and divergence.

The intensity of surface gradients should continue to diminish during winter months and make location of the Alboran front difficult. Figures 10-15 provide evidence that in winter the acoustic front continues to be located on the northern perimeter of the western Alboran gyre and that frontal strength does not vary greatly. Figure 18 is a picture of sea surface temperatures in winter and demonstrates that lack of SST gradients virtually eliminates the ability of DMSP photography to locate the front.

Representative IR photography of Alboran sea surface temperatures in spring is shown in Figure 19. SST gradients are again evident, indicating that surface mixing and cooling are no longer sufficient to obscure the temperature changes produced by the upwelling of colder bottom water.

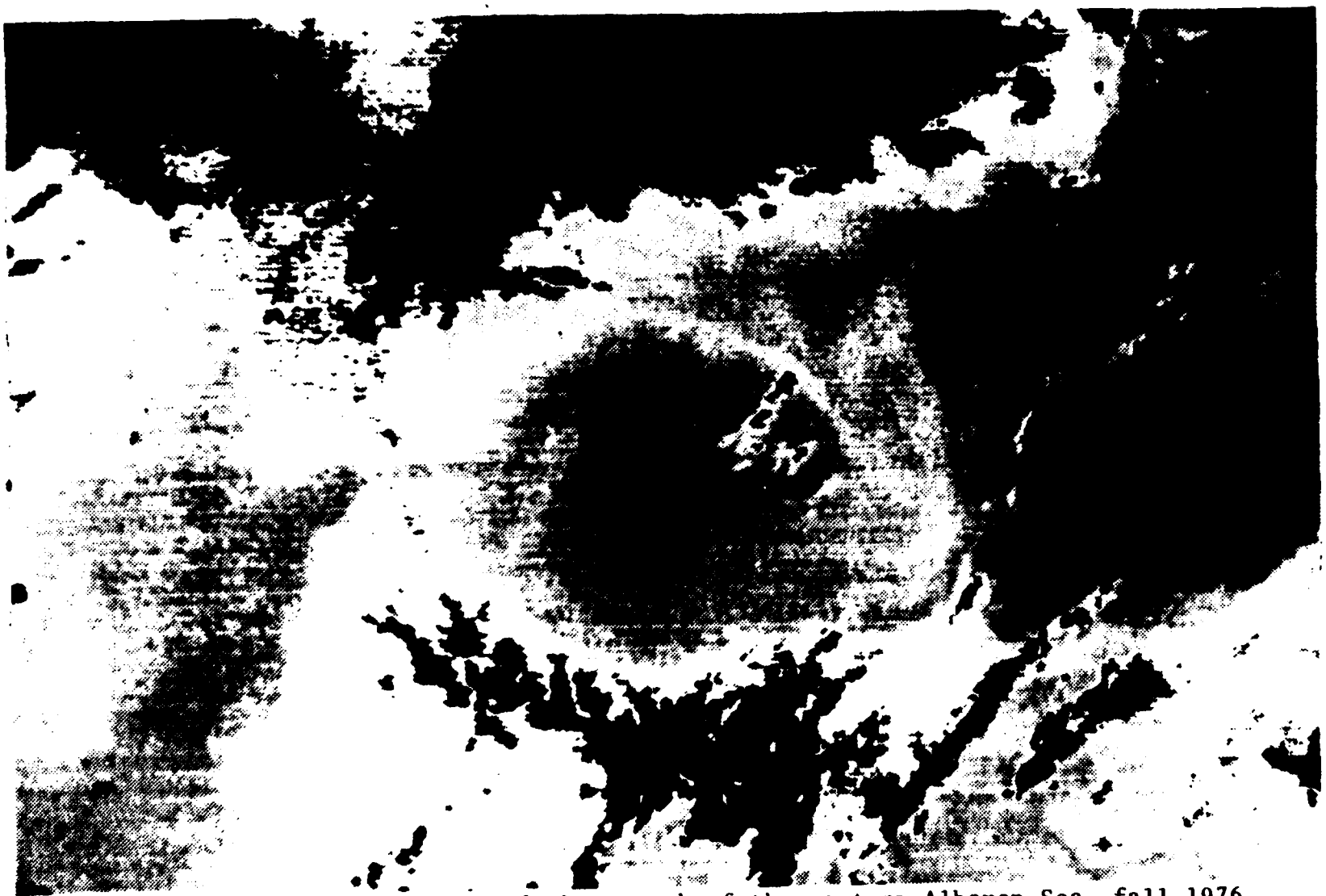

Figure 17. DMSP infrared photograph of the western Alboran Sea, fall 1976. Lighter shading indicates cooler sea surface temperatures.

Figure 18. DMSP infrared photograph of the western Alboran Sea, winter 1977. Lighter shading indicates cooler sea surface temperature.

Figure 19. DMSP infrared photograph of the western Alboran Sea, spring 1977. Lighter shading indicates cooler sea surface temperatures.

It therefore seems evident that DMSP infrared photography can indicate the location of the Alboran acoustic front for a large proportion of the year, a result that can be of practical importance to ASW aircrews operating in the Alboran Sea.

C. ACOUSTIC PROPAGATION

Acoustic propagation conditions in the western Alboran Sea were investigated for the summer and winter seasons for sources located along a potential submarine transit lane. The source locations were as follows:

Position 1 -- 36°-07'N 3°28'W

Position 2 -- 36°-05'N 4°-12'W

Position 3 -- 36°-02'N 4°-44'W

The source positions are plotted on the SLD and SCD maps in Figures 5-15 and identified by encircled position numbers.

Sound speed profiles were calculated from oceanographic observations of the western Alboran Sea for each season and propagation path of interest. These data are presented in Figures 20a through 32a as sound speed cross-sections with isotachs plotted in 5 m/sec increments.

The raytrace displays produced by the RP-70 JCRAYB program are shown in Figures 20b through 32b. These diagrams are intended to illustrate acoustic transmission paths and are not reproductions of the acoustic ray plots used by the RP-70 program to compute propagation loss. The complexity of the complete PL ray plot would obscure important sound path features, making it impractical for illustration.

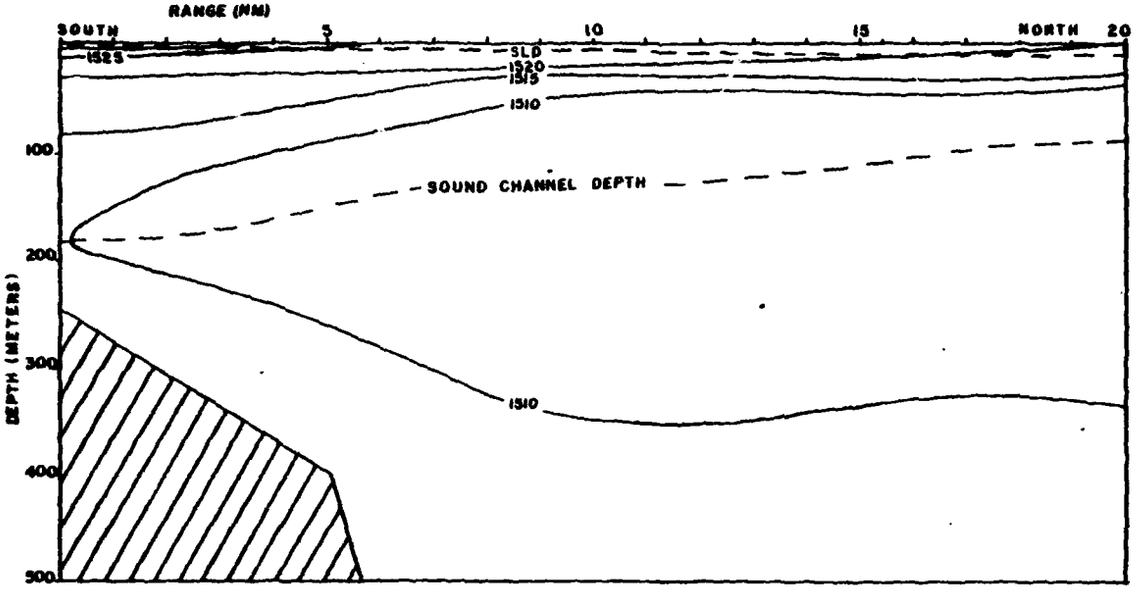

Figure 20a. Sound speed cross-section northward from Position 1, summer 1969 (m sec^{-1}).

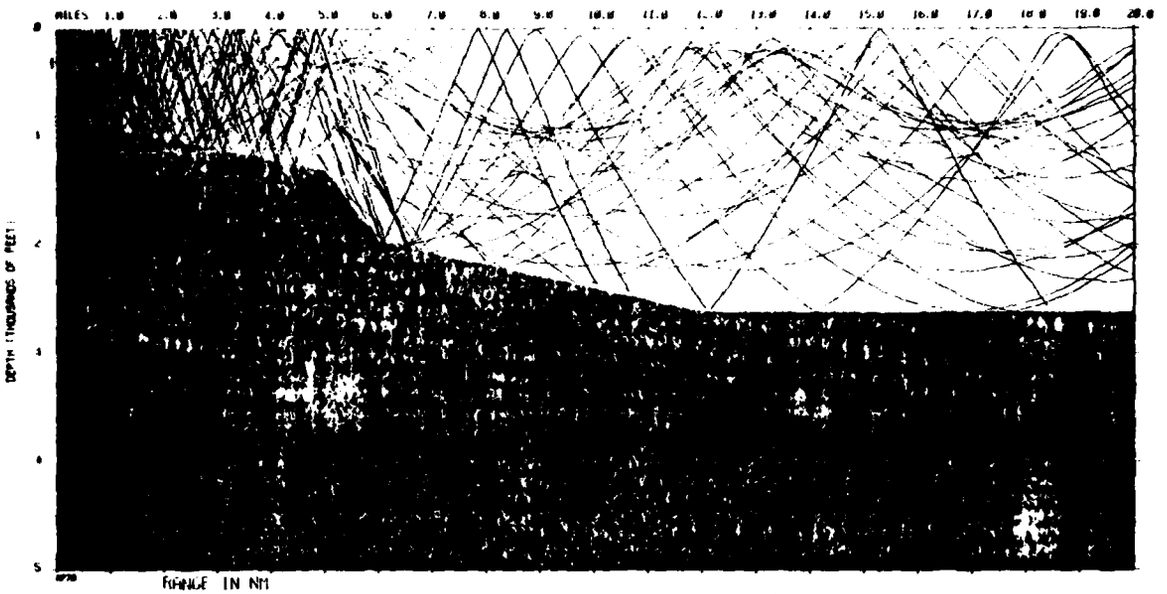

Figure 20b. Raytrace northward from Position 1. Aperture ± 89°.

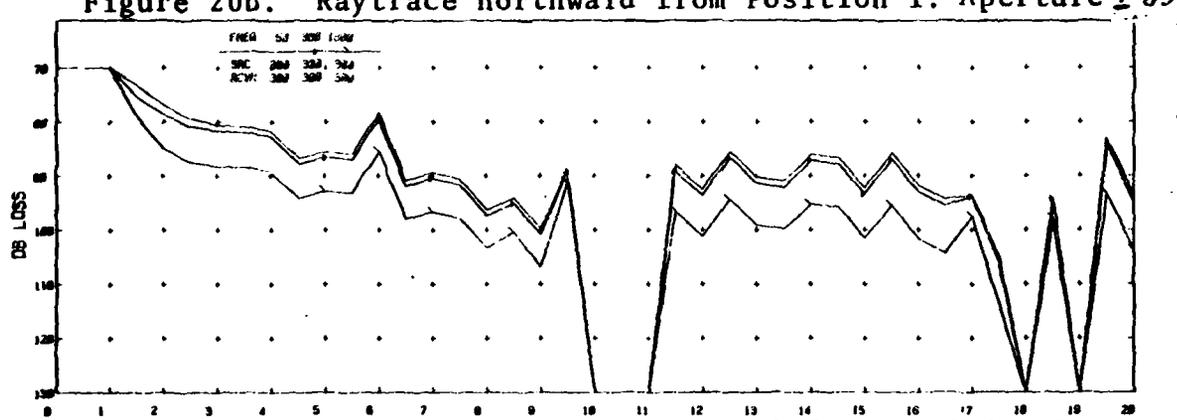

Figure 20c. Propagation loss northward from Position 1.

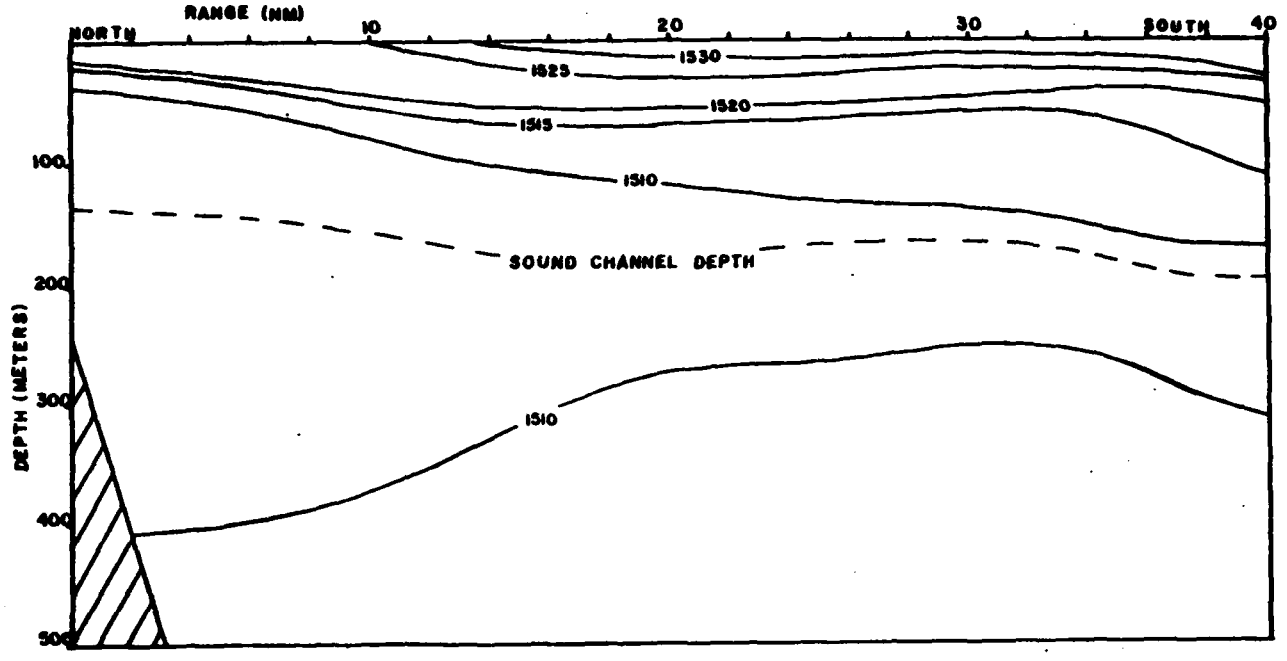

Figure 21a. Sound speed cross-section southward from Position 1, summer 1970 (m sec^{-1}).

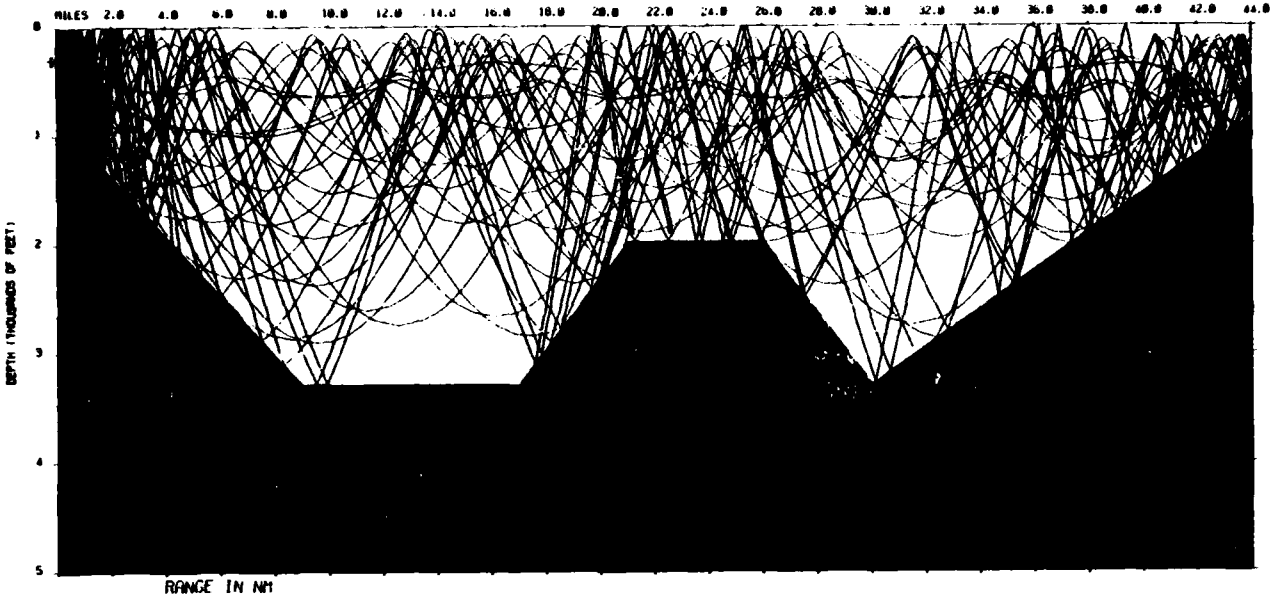

Figure 21b. Raytrace southward from Position 1, Aperture + 89°.

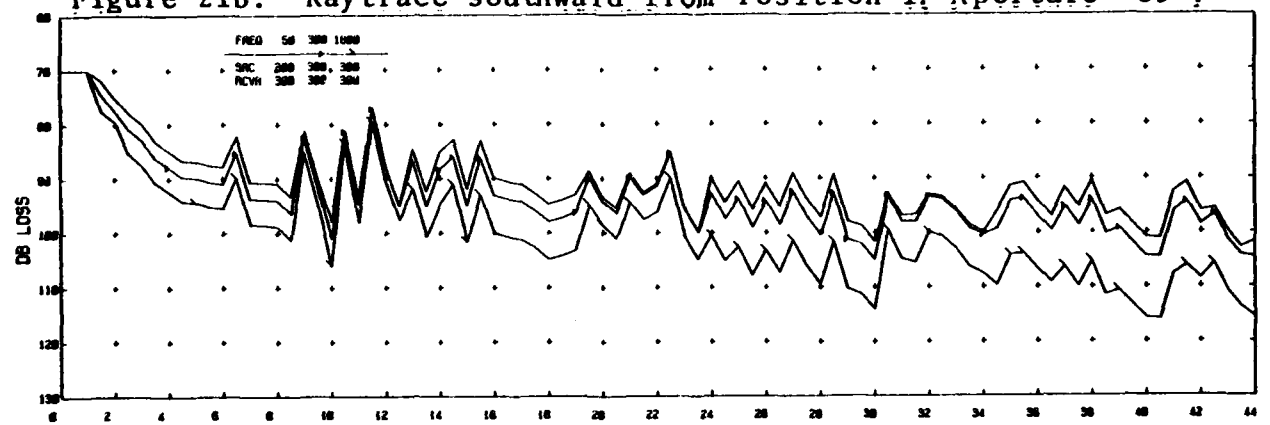

Figure 21c. Propagation loss southward from Position 1.

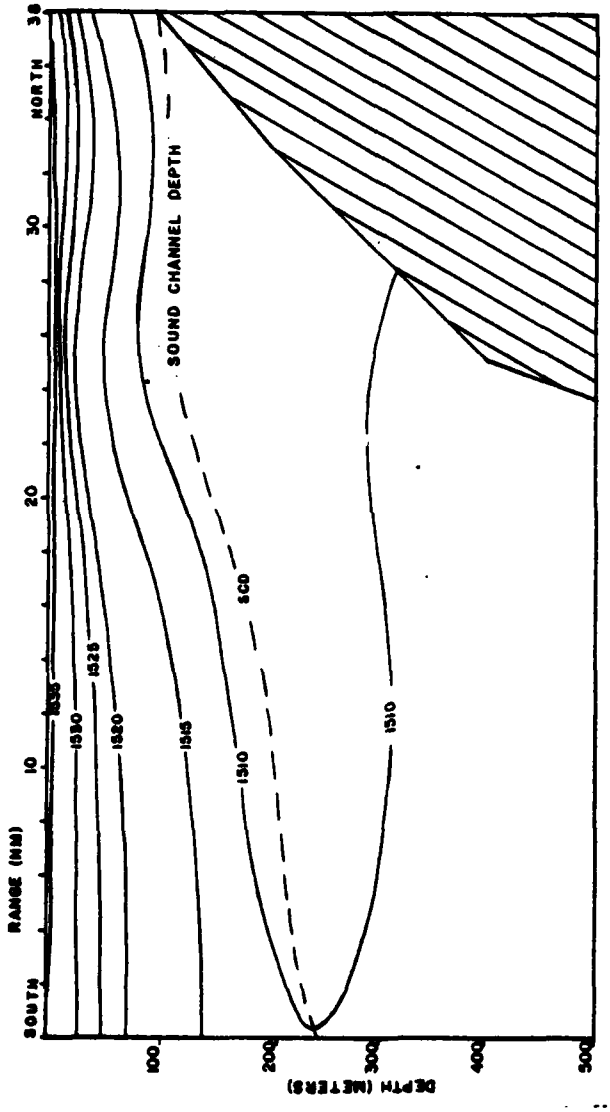

Figure 22a. Sound speed cross-section northward from Position 2, summer 1962 (m sec^{-1}).

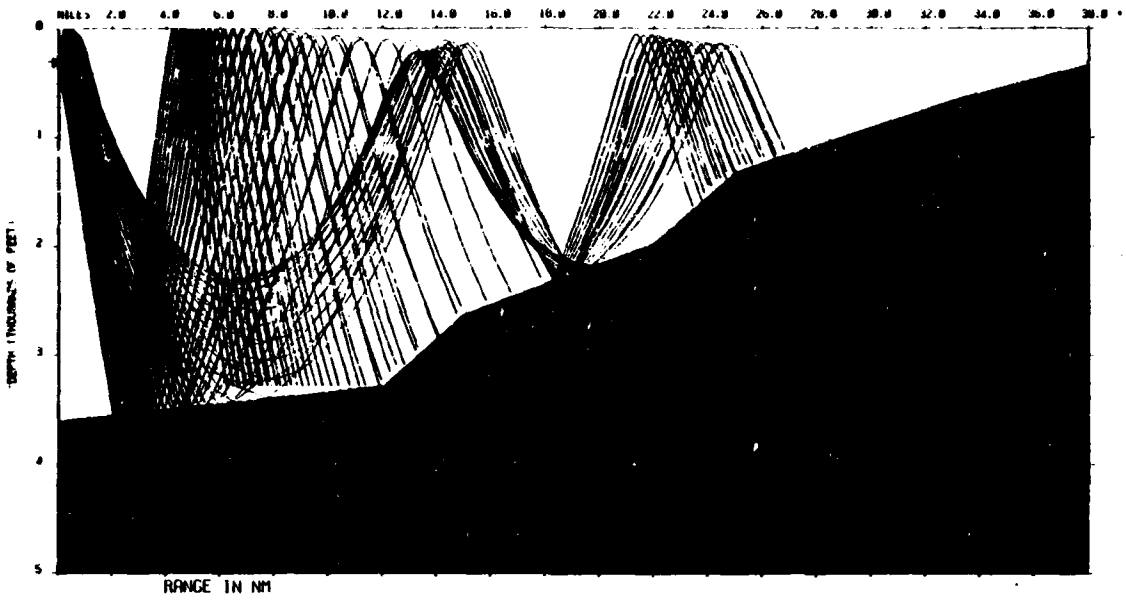

Figure 22b. Raytrace northward from Position 2. Aperture ± 14.5°.

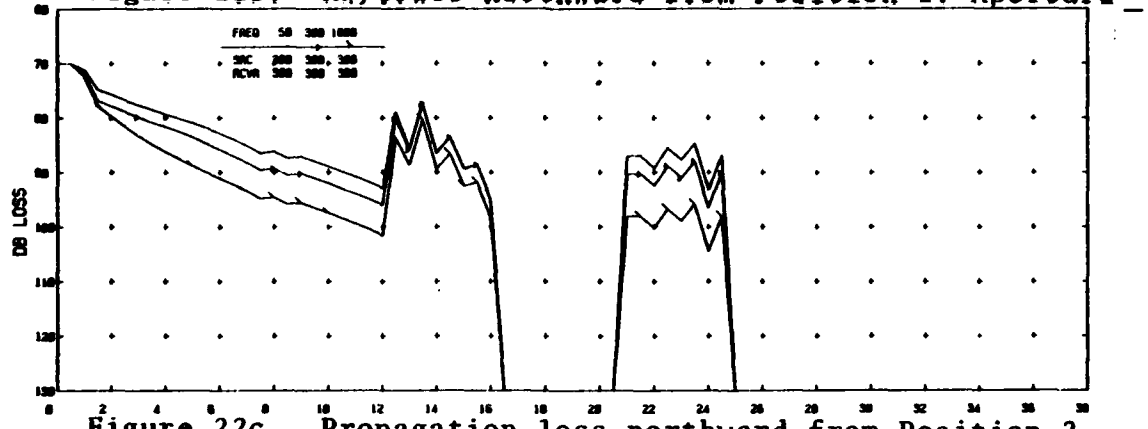

Figure 22c. Propagation loss northward from Position 2.

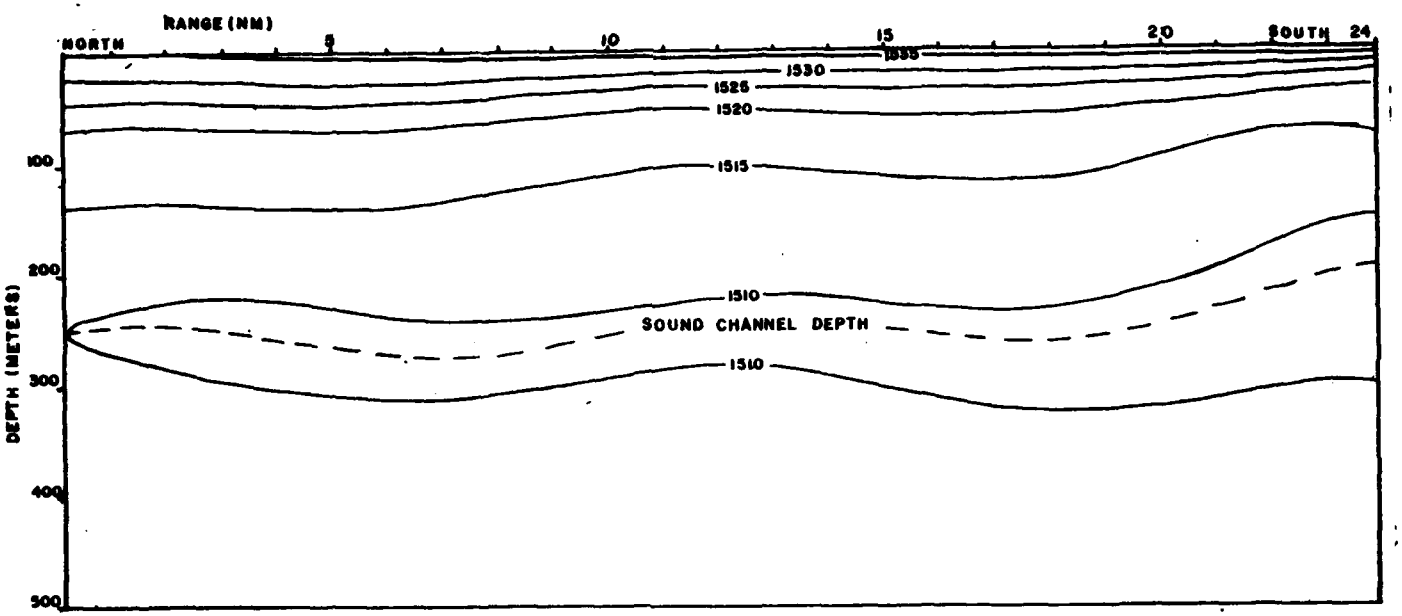

Figure 23a. Sound speed cross-section southward from Position 2, summer 1962 (m sec^{-1}).

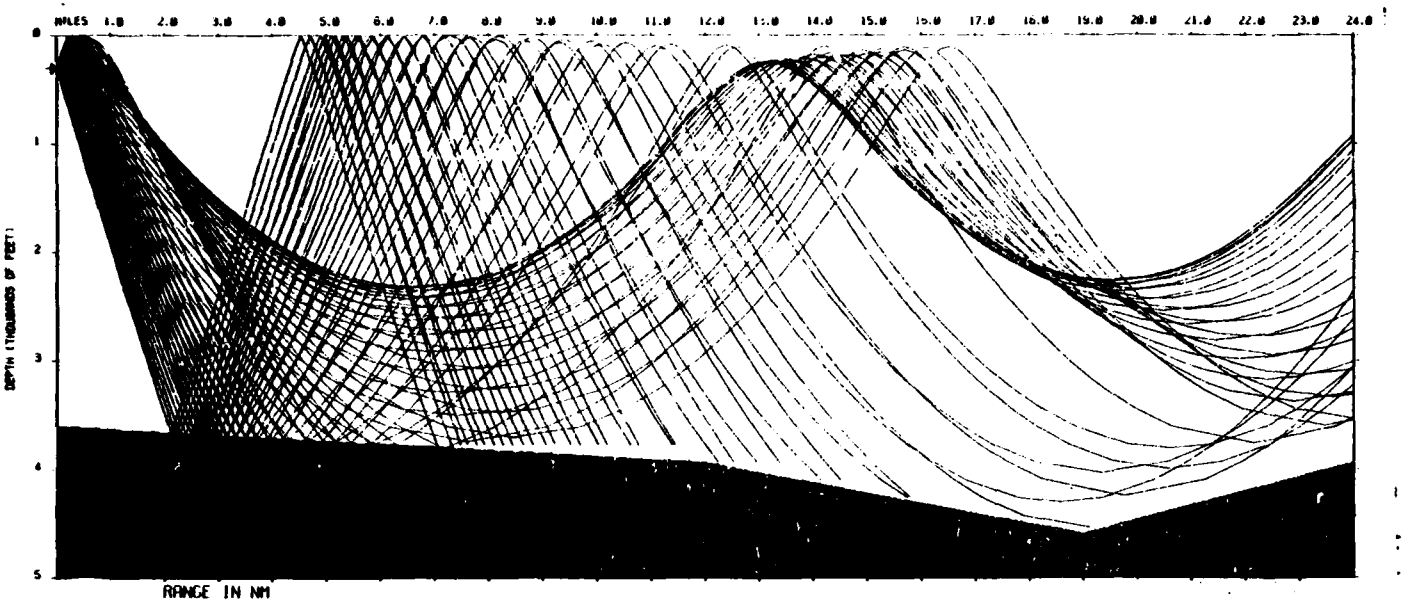

Figure 23b. Raytrace southward from Position 2. Aperture ± 14.5°.

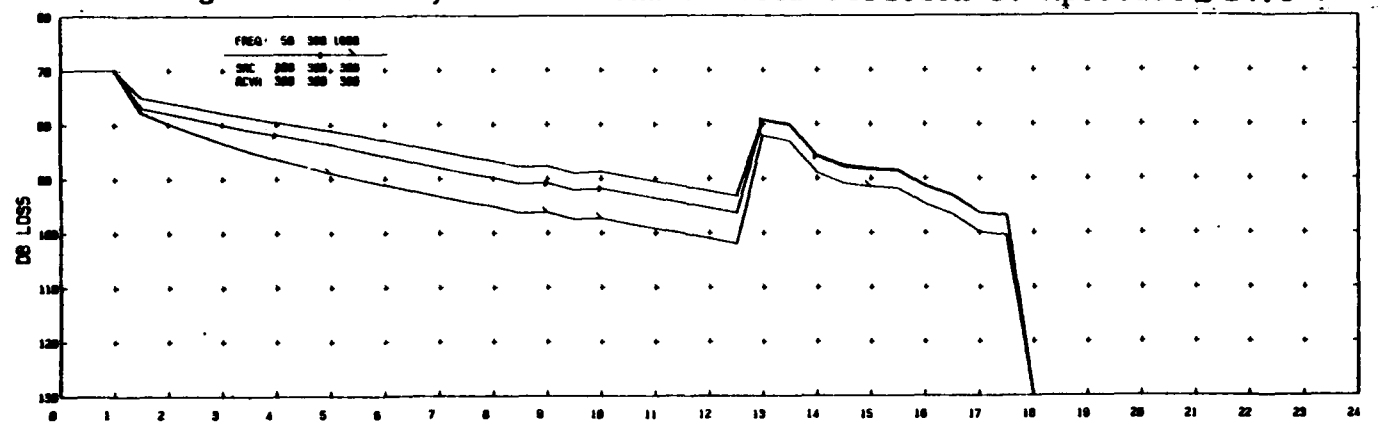

Figure 23c. Propagation loss southward from Position 2.

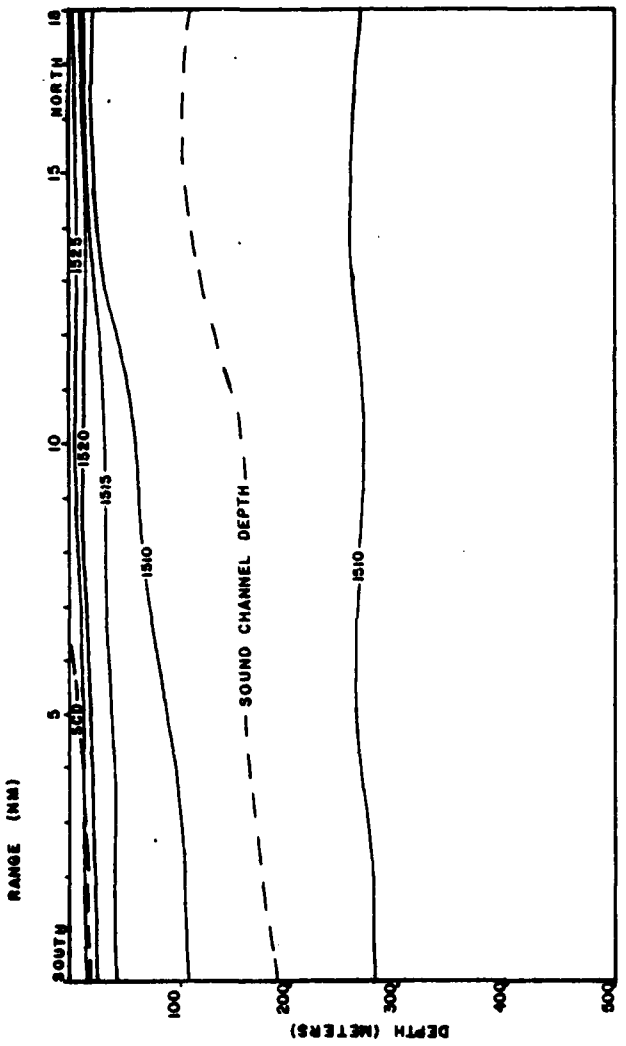

Figure 24a. Sound speed cross-section northward from Position 3, summer 1975 ($m\ sec^{-1}$).

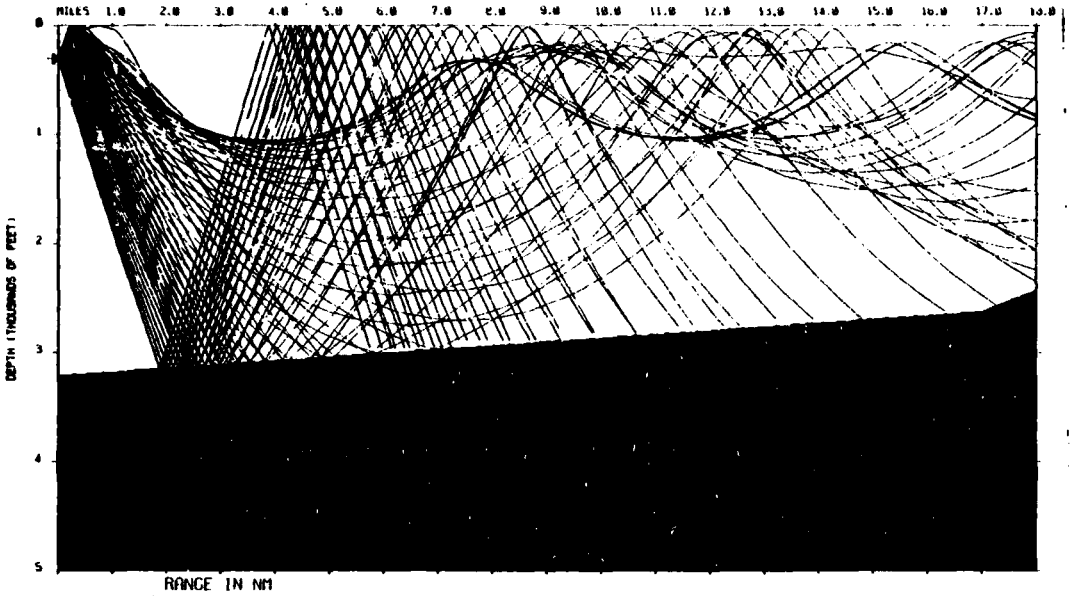

Figure 24b. Raytrace northward from Position 3. Aperture ± 14.5°.

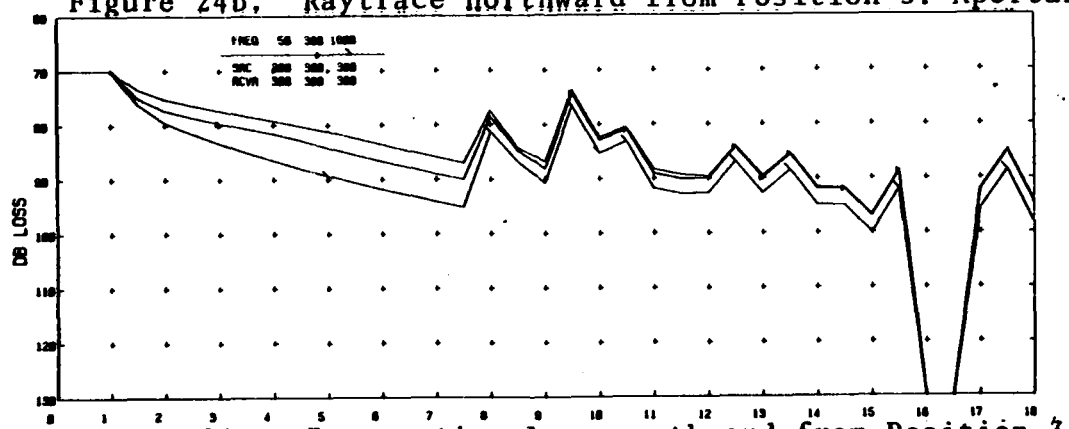

Figure 24c. Propagation loss northward from Position 3.

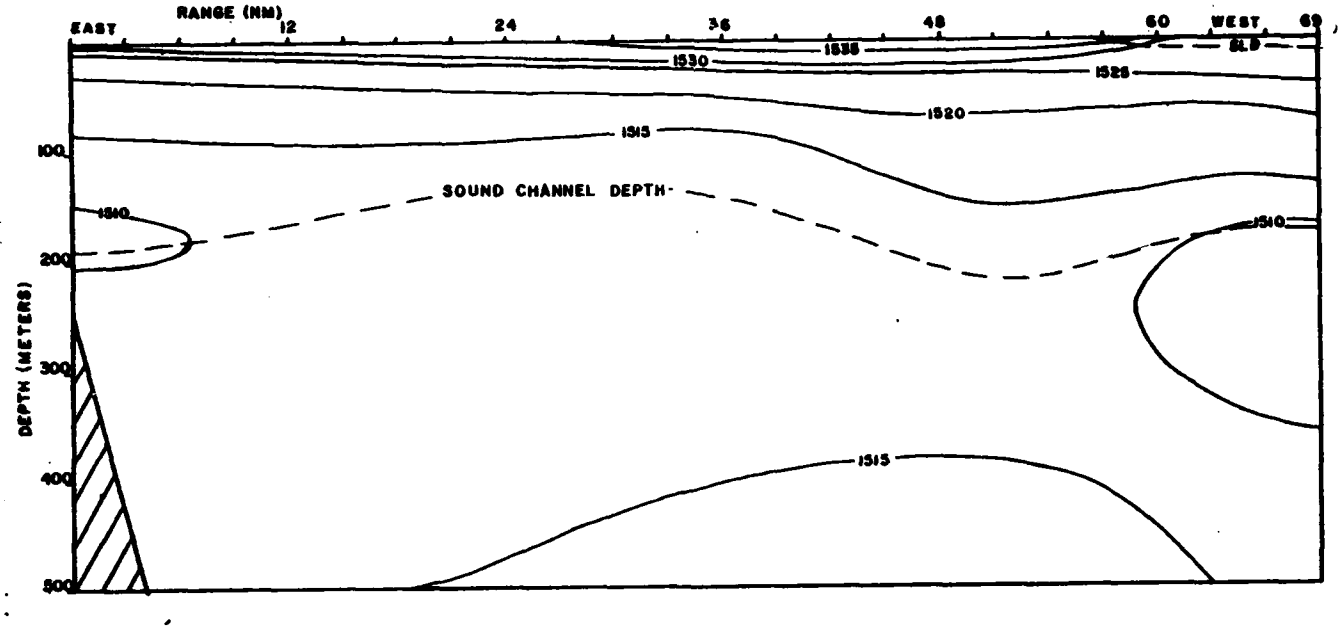

Figure 25a. Sound speed cross-section westward from Position 1, summer 1969 (m sec^{-1}).

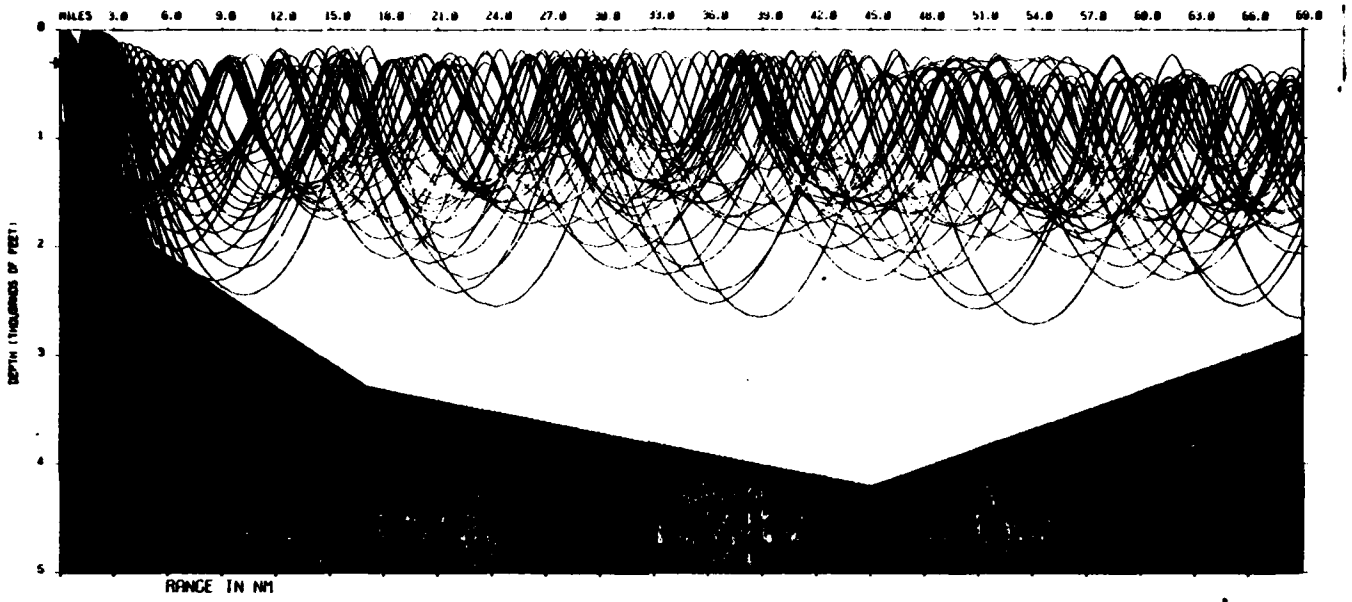

Figure 25b. Raytrace westward from Position 1. Aperture ± 14.5°.

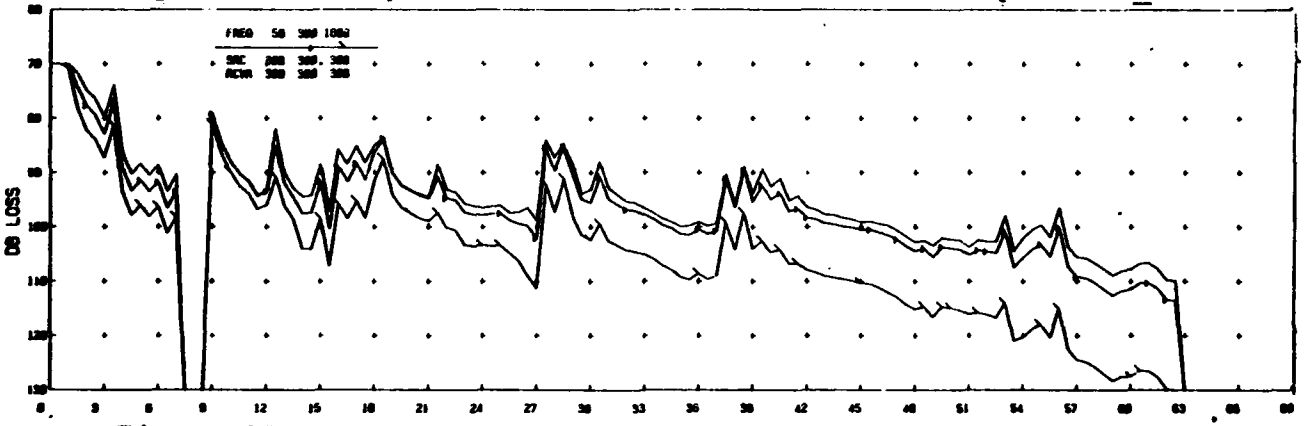

Figure 25c. Propagation loss westward from Position 1.

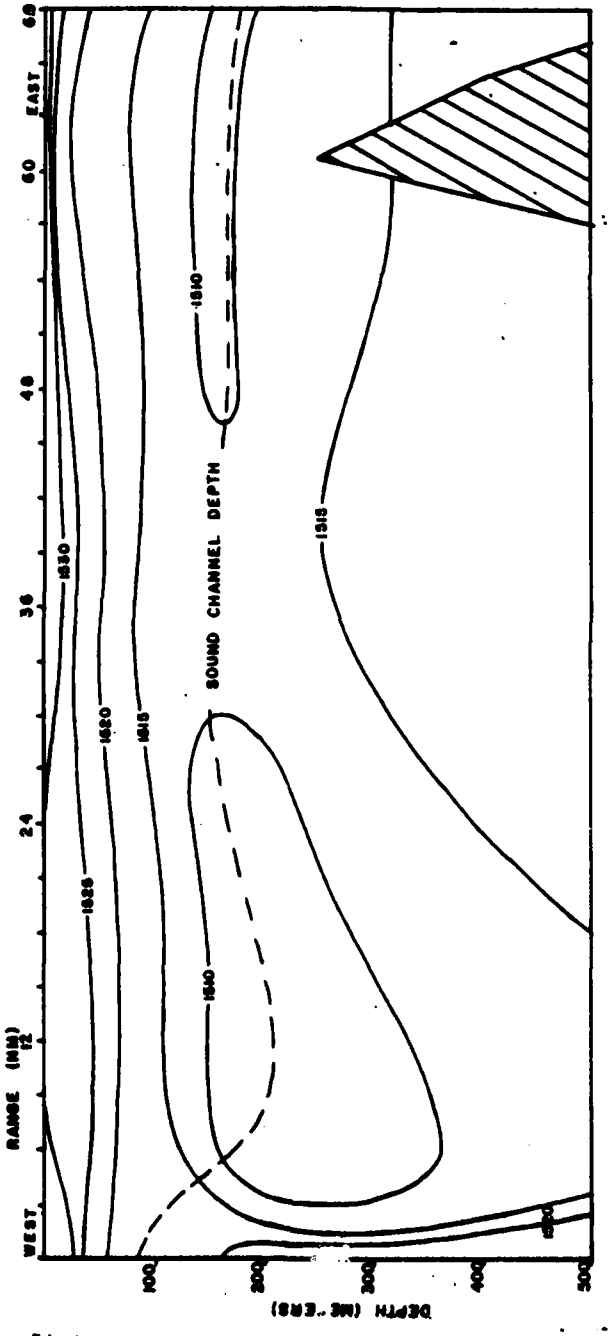

Figure 26a. Sound speed cross-section eastward from Positon 3, summer 1969 (m sec^{-1}).

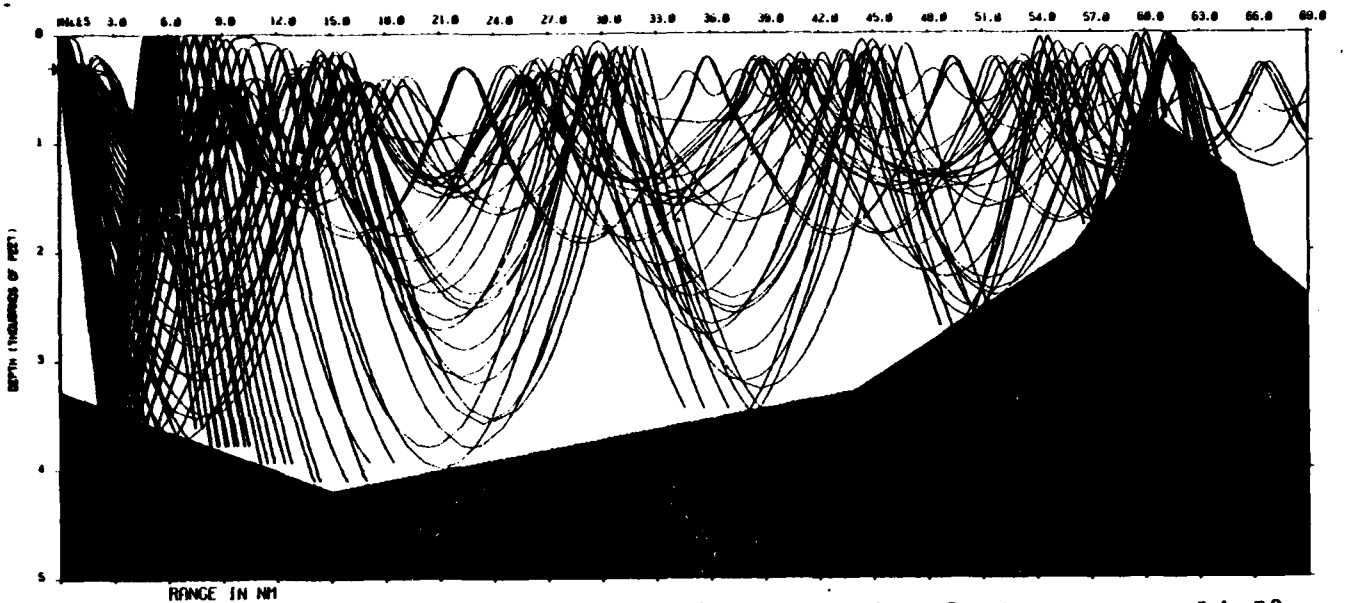

Figure 26b. Raytrace eastward from Position 3. Aperture ±14.5°.

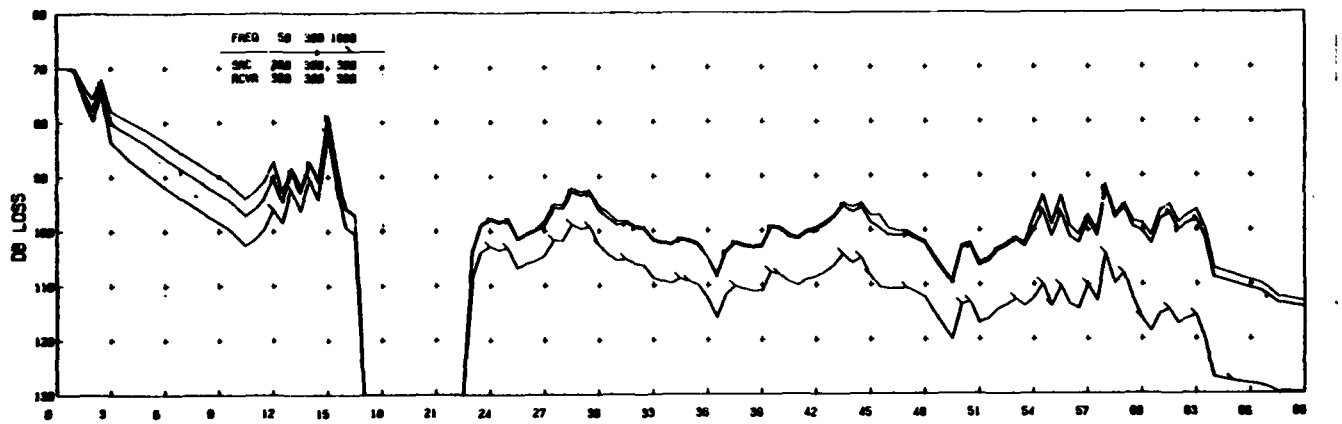

Figure 26c. Propagation loss eastward from Position 3.

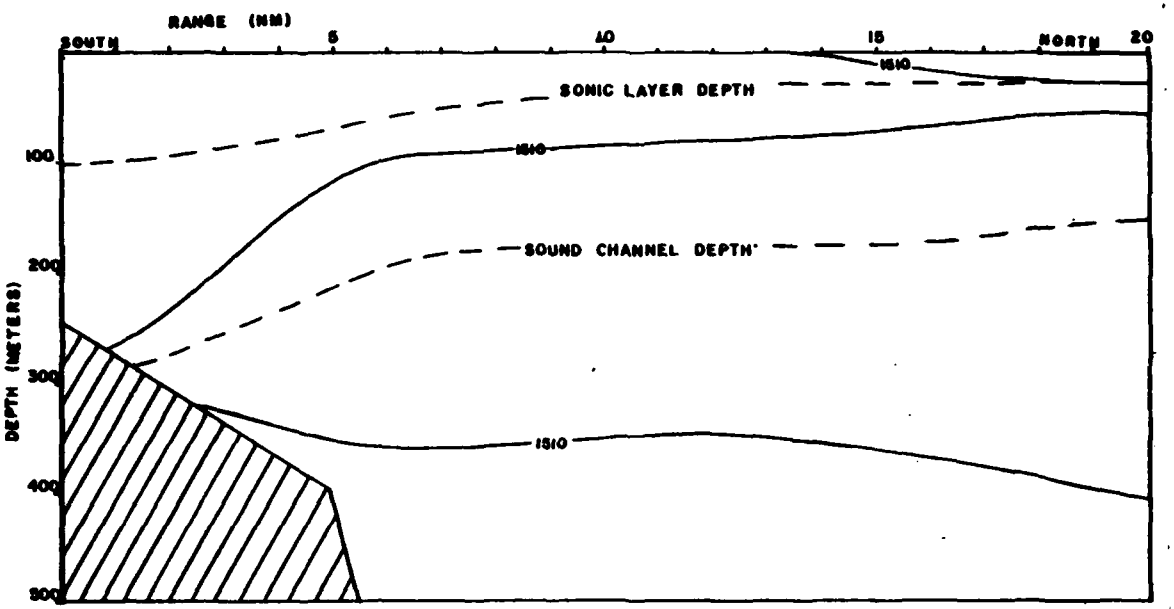

Figure 27a. Sound speed cross-section northward from Position 1, winter 1948 (m sec^{-1}).

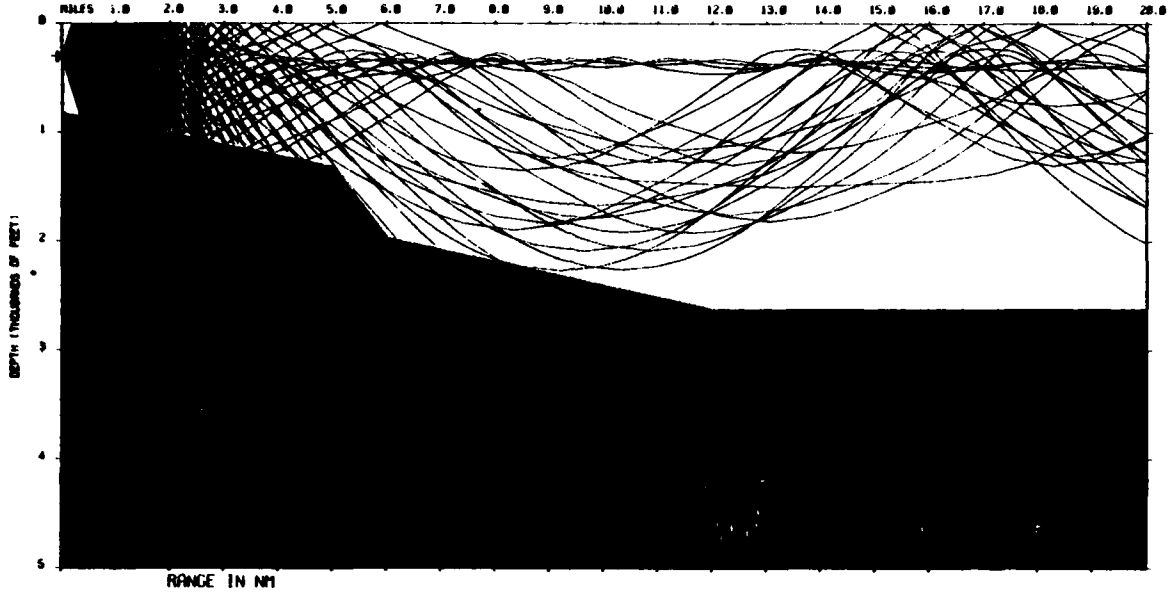

Figure 27b. Raytrace northward from Positon 1. Aperture ± 14.5°.

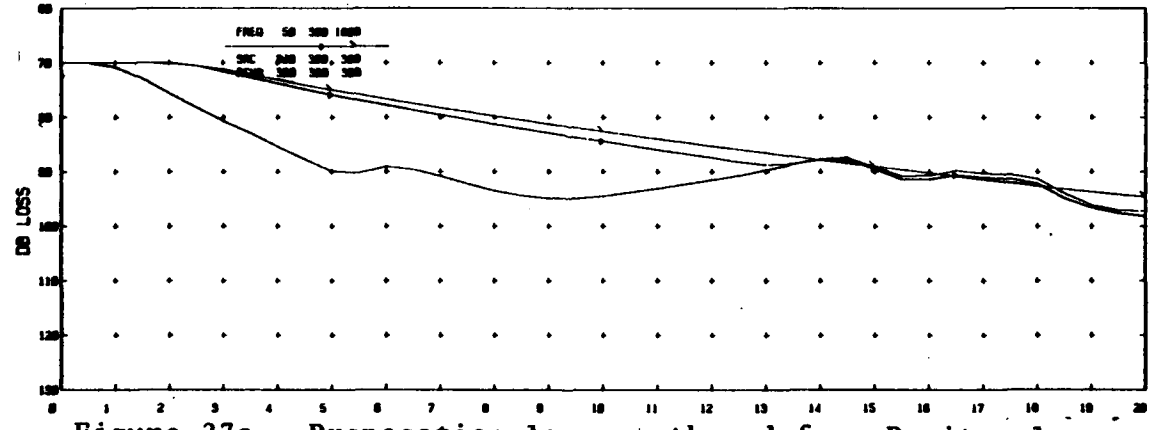

Figure 27c. Propagation loss northward from Positon 1.

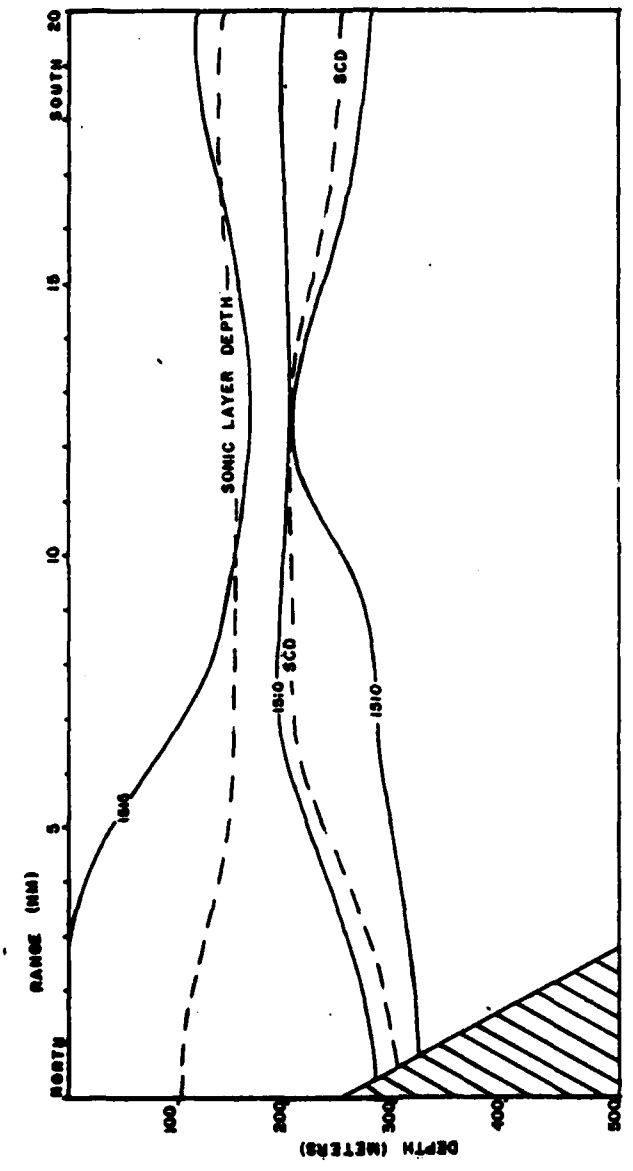

Figure 28a. Sound speed cross-section southward from Position 1, winter 1948 (m sec^{-1}).

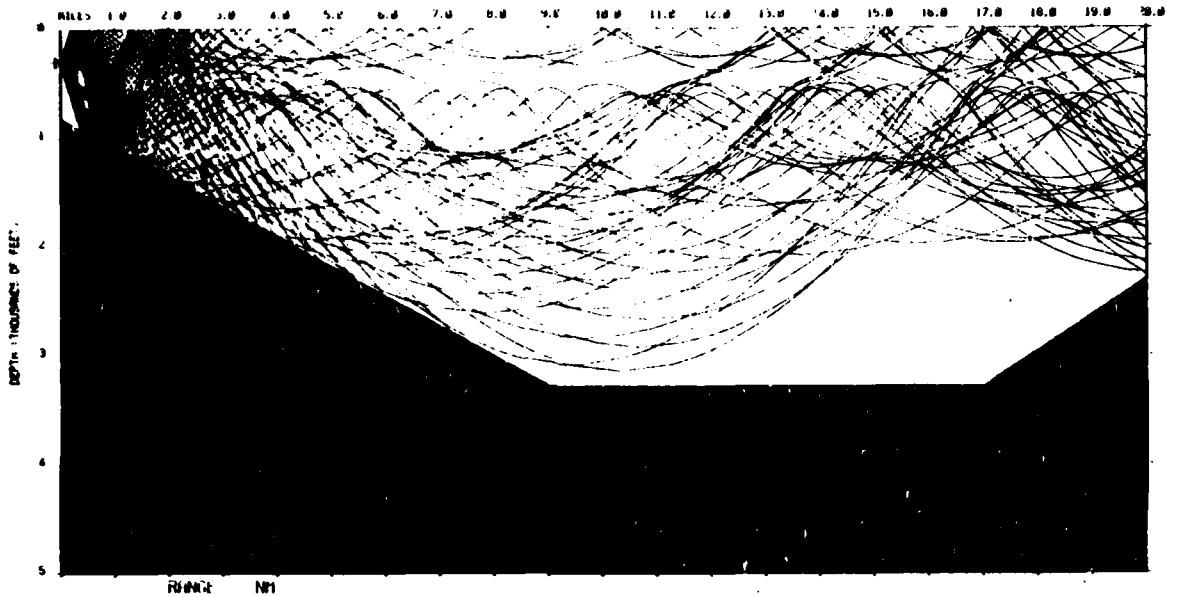

Figure 28b. Raytrace southward from Position 1. Aperture ± 14.5°.

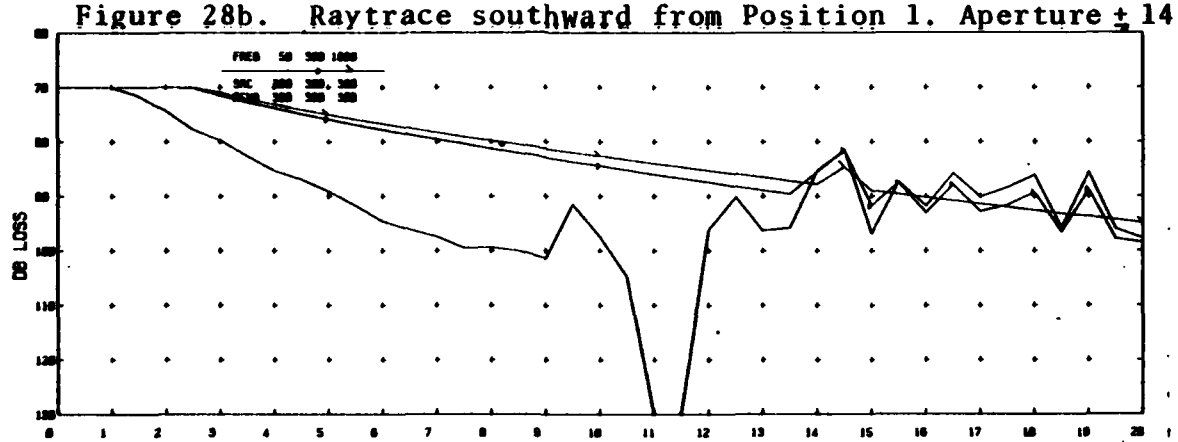

Figure 28c. Propagation loss southward from Position 1.

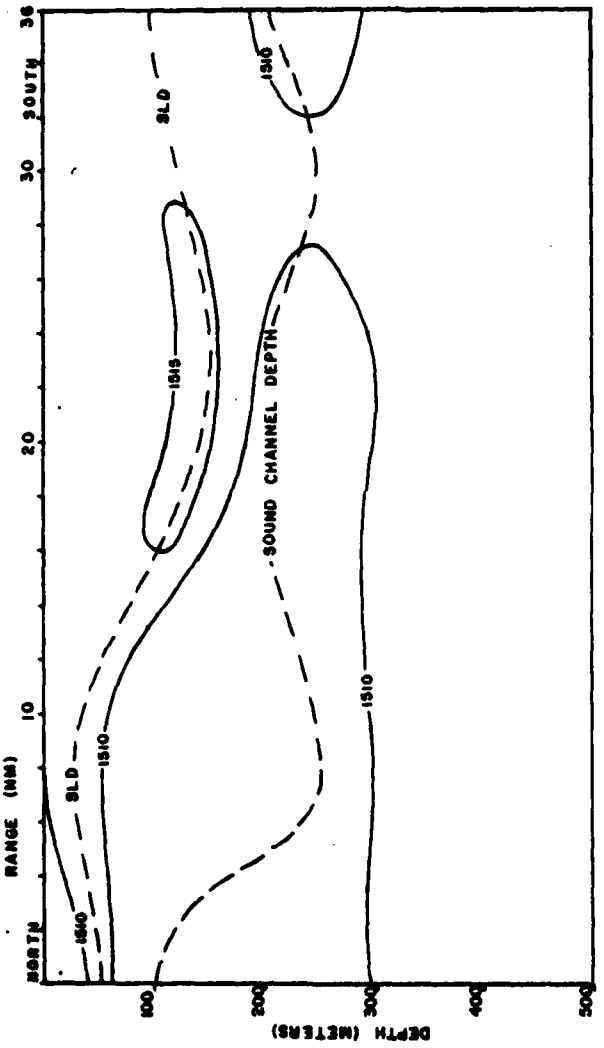

Figure 29a. Sound speed cross-section southward from Position 2, winter 1948 (m sec^{-1}).

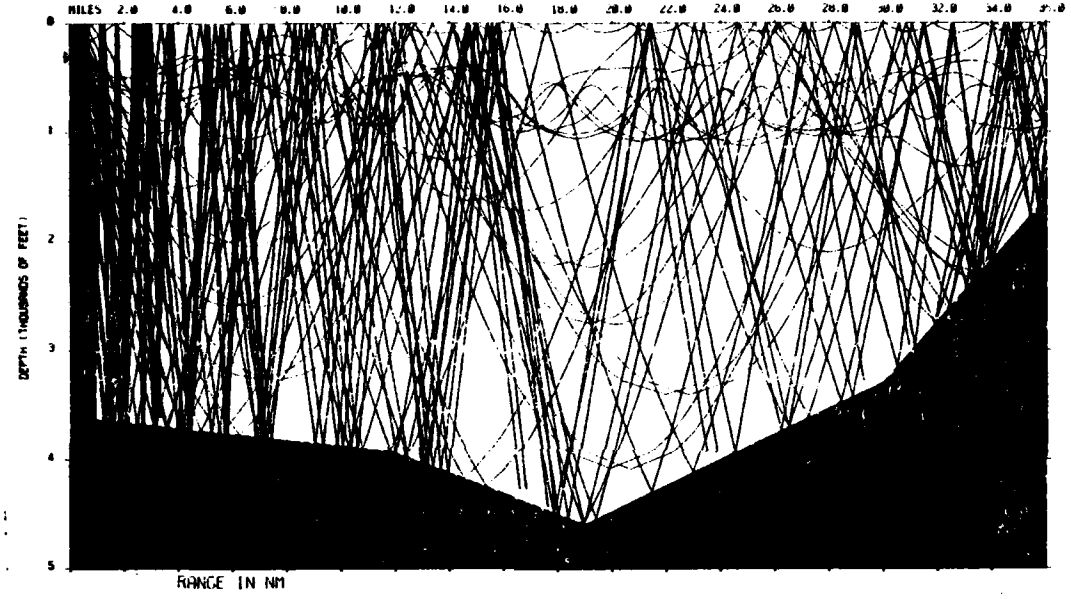

Figure 29b. Raytrace southward from Position 2. Aperture ± 89°.

Figure 29c. Propagation loss southward from Position 2.

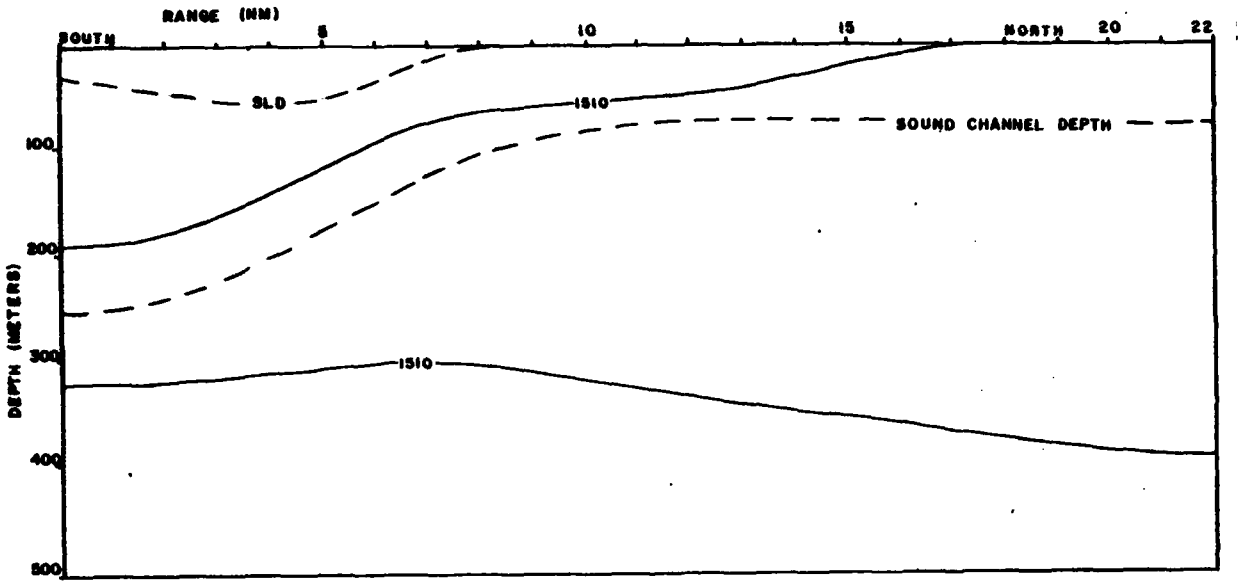

Figure 30a. Sound speed cross-section northward from Position 3, winter 1948 (m sec^{-1}).

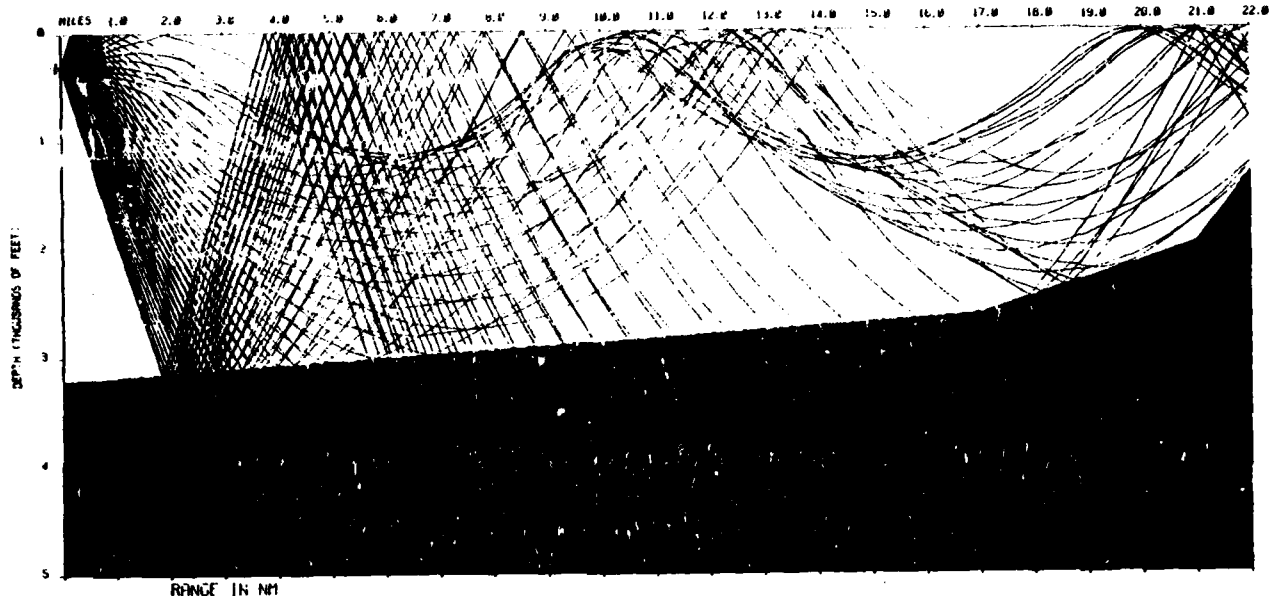

Figure 30b. Raytrace northward from Position 3. Aperture ± 14.5°.

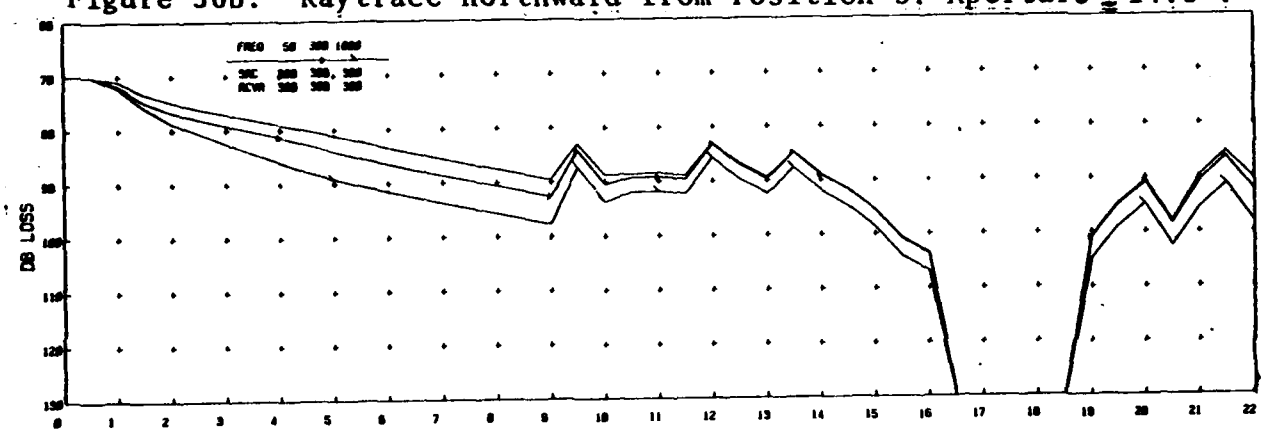

Figure 30c. Propagation loss northward from Position 3.

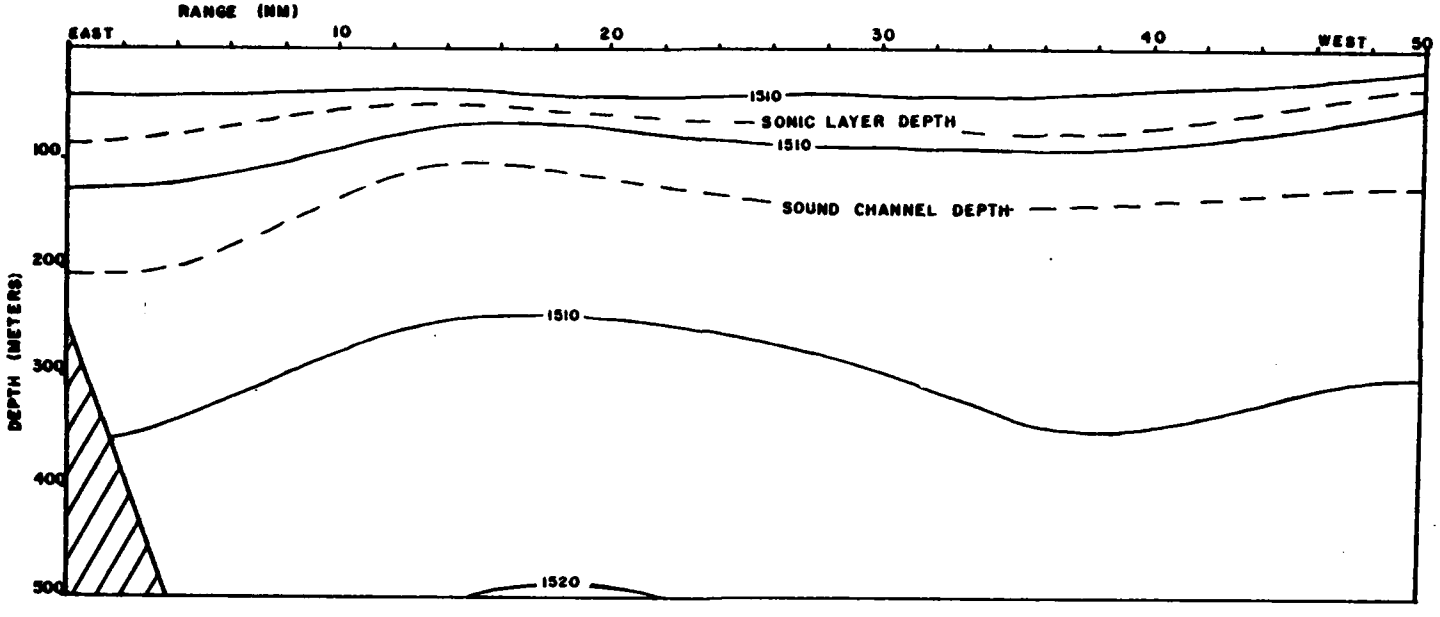

Figure 31a. Sound speed cross-section westward from Position 1, winter 1971 (m sec^{-1}).

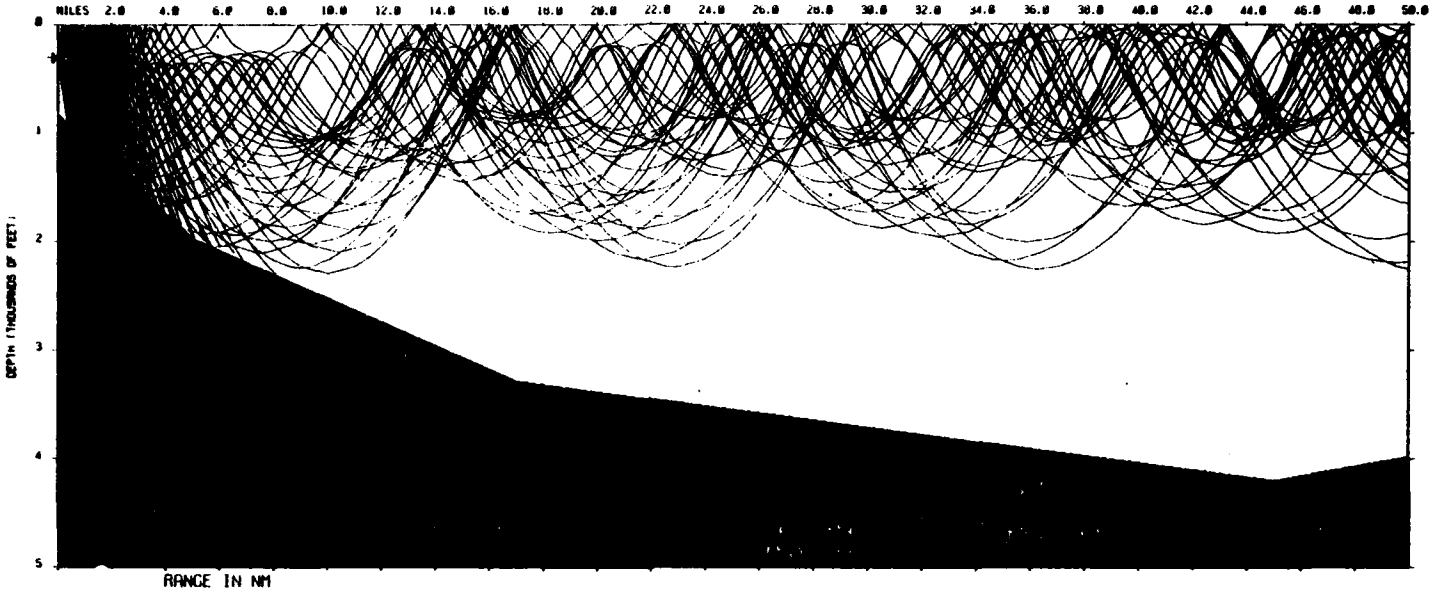

Figure 31b. Raytrace westward from Position 1. Aperture ± 14.5°.

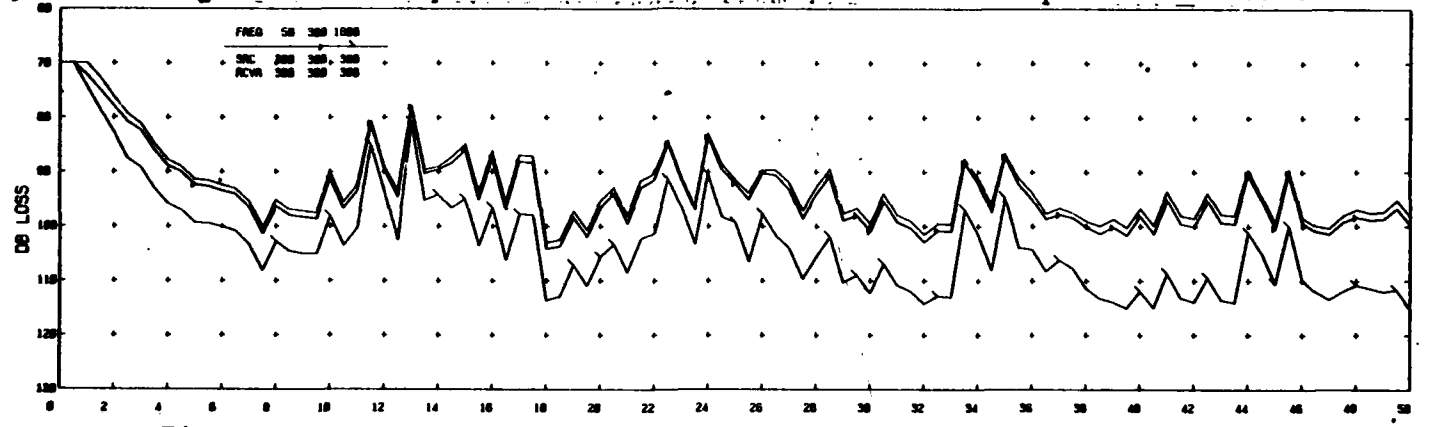

Figure 31c. Propagation loss westward from Position 1.

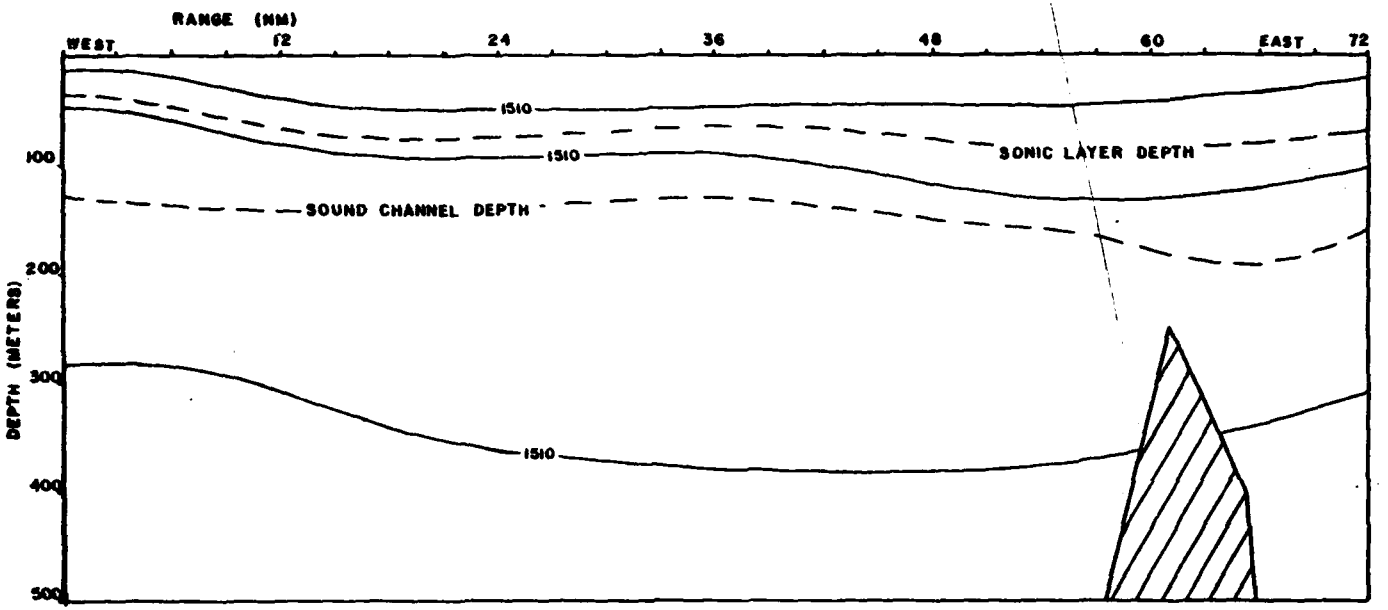

Figure 32a. Sound speed cross-section eastward from Position 3, winter 1971 (m sec^{-1}).

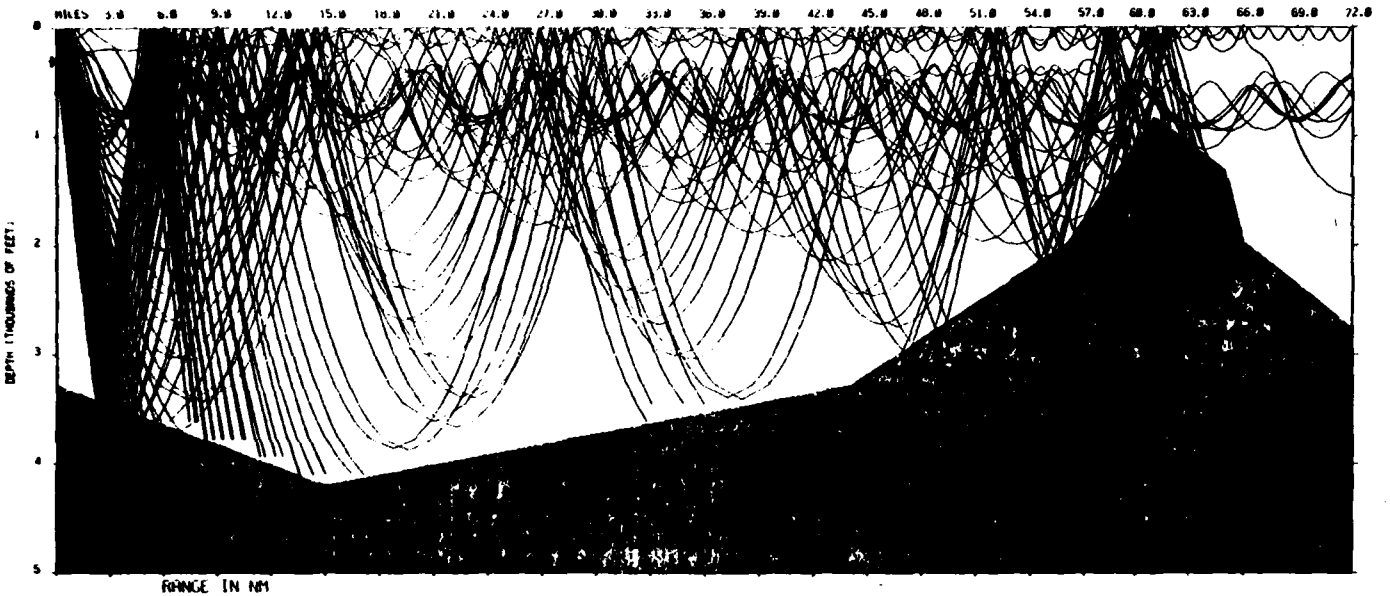

Figure 32b. Raytrace eastward from Position 3. Aperture +14.5°.

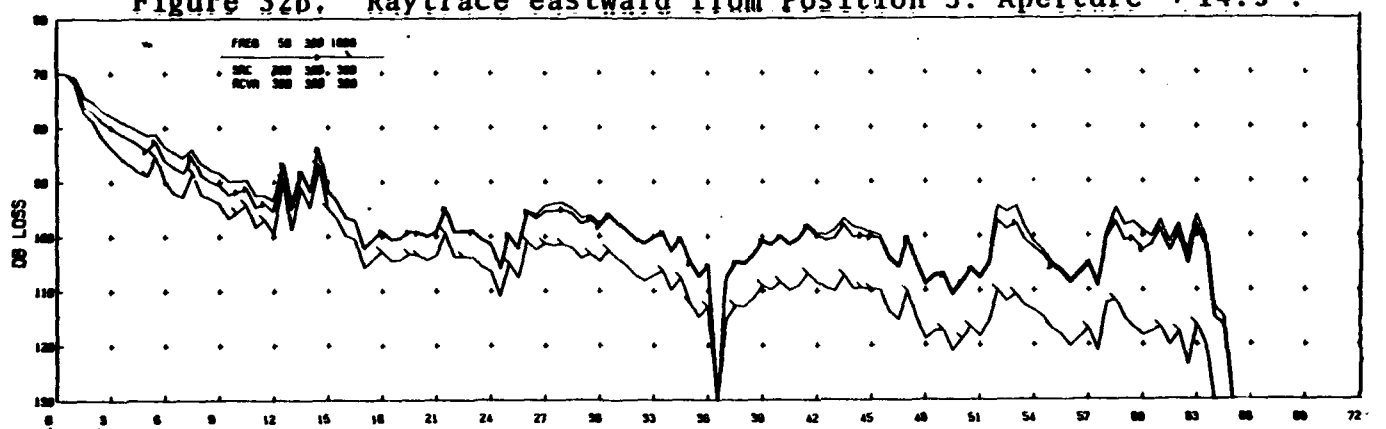

Figure 32c. Propagation loss eastward from Position 3.

Dominant sound transmission paths were best depicted in the raytrace diagram by altering the size of the source aperture. Transmission directions in which acoustic propagation is strongly influenced by bottom and/or surface reflection were illustrated by setting the source operation at $\pm$89°. Directions in which acoustic energy propagated primarily without boundary reflection were illustrated by raytrace diagrams with the aperture restricted to $\pm$14.5°. Raytrace diagram clarity was improved by placing restrictions on the number of rays traced.

The propagation loss curves generated by the RP-70 program were calculated for both source and receiver located at 100 m, and a full aperture coverage ($\pm$ 90°). These curves are presented as Figures 20c through 32c.

1. Summer Propagation

The acoustic propagation path shown in Figure 20 is northward from source Position 1. This position is normally located north of the front and sound energy projected to the north is entirely within the northern acoustic regime. The raytrace diagram in Figure 20b shows the dominant effect of the shallow water at this source position. All sound energy beyond 4 nm travels via a bottom and/or surface reflected path into the sound channel. The result is a non-uniform energy distribution in the sound channel and high attenuation outside the channel.

The propagation loss levels shown in Figure 20c illustrate the strong influence of bottom losses. The increasing

PL near the source reflects the energy losses resulting from multiple bottom reflections while the energy peaks at 6.5 nm and 9.5 nm correspond to single bottom reflections reinforced by sound channel focusing. The extreme changes in propagation loss at 10 - 11 nm and 18 - 19 nm can be attributed to the periodicity of both sound channel focusing and bottom reflection. Thus, it should be expected that sound transmission in summer northward from Position 1 will be dominated by bathymetry.

Acoustic energy propagating southward from Position 1 is shown by Figure 21. Although in summer this transmission path would be expected to cross the Alboran front, inspection of the sound speed cross-section of Figure 21a shows that the increase in sound channel depth is too gradual to qualify as a front. The raytrace and PL diagrams in this figure show that propagation southward from Position 1 is also affected by the shallow water. Yet, unlike northward propagation from this position, most energy enters the sound channel without experiencing bottom reflection, producing a more uniform distribution of energy in the sound channel. The gradual deepening of the SCD shown in Figure 21a produces a reduction of energy at the 100 m depth hydrophone and increases propagation loss with peaks occurring where refracted energy reinforces reflected sound.

Figure 22 shows sound propagation northward from Position 2 in summer. Here a front is located immediately north of the source where a rapidly decreasing SCD is apparent. Water depth at Position 2 is sufficient to permit formation of

a convergence zone; however, the acoustic front tends to reduce the focusing of CZ energy near the surface and the dominant propagation feature is bottom reflection and truncation of the CZ limiting ray by the upsloping bottom. It is also important to note that the changes in sound speed with depth, shown in Figure 22a, are not intense enough to trap low frequency acoustic energy near the sound speed axis.

Figure 23 represents summer acoustic conditions and transmission southward from Position 2 within the western Alboran gyre. The sound speed cross-section in Figure 23a shows that the SCD is almost constant at greater than 200 m. Water depth is sufficient to permit CZ formation and, as noted for transmission northward from Position 2, the sound channel is too weakly focused to trap sound near the sound speed maximum. Thus, the propagation loss diagram of Figure 23c shows energy gains at the CZ annuli followed by rapidly increasing propagation loss.

Figure 24 illustrates sound transmission in summer northward from Position 3. Figure 24a indicates that a significant front is located north of the source position and produces both a shoaling of SLD and a rise in SCD from 180 m to 100 m in less than 20 nm. Although water depth is sufficient for CZ propagation, the rapid shoaling in SCD tends to disrupt CZ formation by decreasing the focusing of CZ energy near the surface and refracting sound into the deep channel. Sound transmission northward through this front also decreases the PL by moving the focus of energy trapped in the sound

channel closer to the hydrophone. This decrease in propagation loss is seen beyond 10 nm range in Figure 24c. Energy gains at about 8 nm and 10 nm range apparent in Figure 24c correspond to reinforcement from CZ and bottom or surface reflected sound. The periodicity of sound channel and CZ focusing combined with bottom absorption of acoustic energy produce a dramatic change in propagation loss level at 16 - 17 nm.

Propagation to the south from Position 3 is not shown since it is entirely within the southern acoustic regime and an almost constant SLD and SCD make the water mass acoustically homogeneous. In this area, sound is transmitted via convergence zone and sound channel paths without frontally induced changes.

Sound transmission westward from a source located at Position 1 is illustrated by Figure 25. The shallow water at this position makes bottom reflected energy dominant within the first 5 nm. At longer distances the rapidly increasing depth allows energy to enter the sound channel without bottom reflection. This refracted energy is focused by the sound channel at about 9 nm intervals resulting in the periodic decreases in PL apparent in Figure 25c.

The sound speed cross-section in Figure 25a shows a deepening of the SCD near Gibraltar at about 42 nm range, from 130 m to 220 m over 25 nm. The raytrace and propagation loss diagrams show the effect of this frontal zone. Sound energy in the channel is carried to greater depths, thus

decreasing the acoustic energy available at the 100 m receiver depth and increasing propagation loss. In addition, Figure 25c shows that transmission across an acoustic front tends to disrupt CZ propagation and decrease the focusing of sound energy.

Figure 26a shows that east of the No. 3 source position the summer sound transmission path immediately crosses an acoustic front. The sound speed cross-section depicts a deepening in SCD from 100 m at 2 nm range to 200 m at 12 nm range. This frontal zone corresponds to that shown in Figure 25a at 42 nm range. The strength of this frontal zone close to Gibraltar may be attributed to the narrow, concentrated inflow of Atlantic surface water at the Strait.

The sound propagation path of Figure 26 is parallel to, but opposite in direction to that shown in Figure 25. It was noted in the discussion of Figure 25 that sound traveling westward originates in water too shallow for CZ formation and is reflected or refracted into the sound channel which, near Gibraltar, carries acoustic energy below the receiver depth. In contrast, the acoustic energy shown propagating eastward from Gibraltar in Figure 26 originates in water depths sufficient for CZ formation and is trapped in a sound channel with an axis which gradually rises to near hydrophone depth. Figure 26c shows a large increase in PL from 17 - 23 nm. This energy loss at the hydrophone is a result of a sound channel located well below receiver depth, the uneven distribution of energy in the sound channel, the absence of CZ energy near the surface, and bottom reflection losses.

It is important that ASW aircrews fully appreciate the changes in transmission loss curves resulting from the non-reciprocity of propagation paths through the Alboran front in summer. For energy traveling eastward from Gibraltar the frontal system can virtually eliminate CZ focusing after the first convergence zone. At greater distances from Gibraltar the shoaling of the SCD to near hydrophone depth can maintain acoustic energy levels at almost constant values. These effects can be seen in Figure 26.

For sound propagating from the area northwest of Alboran Island toward Gibraltar the energy caustics in the sound channel can produce CZ-like reinforcements of propagation loss, but with the distance between peaks altered as the sound energy transits the frontal zone. In addition, Figure 25 shows that this westward propagating sound is focused at depths increasingly below receiver depth producing a rapid increase in PL over relatively short distances.

2. Winter Propagation

Typical winter acoustic conditions for transmission paths northward and southward from source Position 1 are illustrated by Figures 27 and 28. These figures show that in winter, like the summer conditions illustrated in Figures 20 and 22, propagation from the shallow water at Position 1 to deep water is strongly influenced by bottom reflected paths. In summer a large part of the projected energy entered the sound channel via bottom reflected paths, while in winter a significantly increased proportion of sound is refracted directly into the

channel without bottom loss. This seasonal change in propagation pattern is largely responsible for the lower transmission losses seen in Figures 27c and 28c.

Figure 27a shows an acoustic front located about 5 nm north of Position 1. As in summer, the presence of the front has little impact on propagation from this shallow area. A highly focused sound channel traps 300 Hz and 1800 Hz sound at the axis, maintaining almost constant PL levels. 50 Hz energy is not as efficiently trapped and shows the influence of CZ formation. Figure 27 also illustrates the effect of the shallow, weak surface duct typically found in winter over the northern acoustic regime. The figure shows that sound is not trapped near the surface, but is refracted into the deep sound channel.

Figure 28 illustrates propagation in winter, south of the acoustic front. The figure shows that the sonic layer depth has increased to about 150 m, trapping 300 Hz and 1800 Hz sound in a deep surface duct and improving propagation loss from summer levels. This winter improvement in PL for a 100 m receiver is illustrated by comparing Figures 21c and 28c. It should be noted that, as in summer, 50 Hz sound is refracted into the generally deeper sound channel in the southern acoustic regime, resulting in a peaking of PL in regions of ray convergence and a relatively constant but lower 50 Hz propagation loss level. The rapid decrease in sound energy between 10 nm and 12 nm in Figure 28c is produced by the periodicity of surface duct and sound channel propagation.

Winter acoustic conditions south of Position 2 are represented in Figure 29. Sound transmission northward through the homogeneous northern regime is not shown. A front appears in the sound speed cross-section of Figure 29a immediately south of the source location and, as in summer, marks a change from shallower to deeper SLD and SCD. The effect of these changes can be seen in Figure 29b as the formation of a surface duct at 12 nm and a depth increase for sound transmitted near the sound channel axis. The formation of the surface duct tends to increase the energy available to the hydrophone while the deeper SCD reduces the sound presented to the receiver. The large decrease in the sound energy level seen in Figure 29b between 17 nm and 21 nm can be attributed to the increasing bottom depth and consequent change in the periodicity of bottom reflected energy.

Figure 30 shows winter acoustic conditions northward from source Position 3. The front position shown in Figure 30a is just north of the source location. This frontal location is similar to the summer position pictured in Figure 24a. At source Position 3 water depth is sufficient to allow CZ formation but, as noted in the discussion of Figure 24, the decrease in SLD disrupts CZ focusing and reduces peak energy levels. As in Figure 24, the winter propagation shown in Figure 30 produces energy gains associated with bottom reflection.

Sound propagation westward from Position 1 in winter is shown in Figure 31. In this figure, SLD and SCD shoaling

evident in the sound speed cross-section indicate that a front is located at about 12 mn from the source. Although the shallow water at the source position tends to restrict CZ formation, sufficient energy is transmitted in this mode to produce peaks in the PL diagram. The acoustic front alters the CZ annulus radius from 12.5 nm to 10.5 nm but does not greatly decrease focusing. In addition, Figure 31a shows that west of this front SLD and SCD approach the same depth, producing almost constant PL levels.

The discussion of Figures 25 and 26 pointed out that for propagation through the Alboran front from a region of deep SCD to an acoustic regime where the SCD decreases to near hydrophone depth propagation loss is decreased or held almost constant. Figure 31c illustrates this effect on PL for winter, as well as depicting a front-induced change in CZ radius from 12 nm to 10 nm.

Winter sound propagation to the east from Position 3 is pictured in Figure 32. This path is the reciprocal of westward propagation from Position 1, shown in Figure 31. In these two figures an acoustic front crossing appears near Alboran Island rather than close to Gibraltar, as in the summer conditions illustrated in Figures 25 and 26. However, like Figures 25 and 26, Figures 31 and 32 show changes in PL level resulting from non-reciprocity along propagation paths through the front.

The increase in SLD and SCD near Alboran Island appearing in the sound speed cross-section of Figure 32a

indicates that for almost all of the transmission path, sound is traveling within the nearly homogeneous northern regime. Figure 32b and 32c show that after an initial reinforcement of sound channel and CZ energy by bottom reflection, the PL remains relatively constant and the influence on transmission loss of the upsloping bottom is more pronounced than changes attributed to water mass variations.

D. APPLICATION TO ASW

The preceding discussions of low frequency sound transmission in the western Alboran Sea of the Mediterranean make clear the importance of defining the location of the Alboran front and the horizontal changes it produces in the acoustic environment. Although the descriptions of acoustic propagation were divided into winter and summer seasons, the comparisons drawn suggest that strong, seasonally independent similarities exist for propagation within the northern and southern acoustic regimes. Further, the discussions of sound traveling from one acoustic region to another indicate that non-reciprocity produces changes in propagation loss levels as significant as those attributed to seasonal variations.

It therefore seems reasonable to expect that coupling an understanding of the acoustic effects of the Alboran front with the nearly year-round ability of DMSP infrared photography to depict frontal location can be directly applicable to ASW operations in the eastern approaches to Gibraltar.

IV. CONCLUSIONS

The western Alboran acoustic front appears to be geographically stable, seasonally independent and, for all but the winter season, coincident with sea surface temperature gradients which are detectable by DMSP infrared photography.

The front divides the western Alboran basin into northern and southern acoustic regimes. The northern regime is characterized throughout the year by sonic layer depths (SLD) of less than 50 m and sound channel axis depths (SCD) of about 100 m. In the southern region the SLD is near 150 m in winter and less than 50 m in summer while the SCD is greater than 200 m in all seasons.

Sound energy crossing the front from the northern to the southern acoustic region will generally be refracted downward into the sound channel below a 100 m hydrophone. Sound energy traveling from the southern to the northern acoustic regime will be carried upward toward the 100 m receiver.

The non-reciprocity of acoustic transmission across the front should improve propagation loss levels for a 100 m receiver located north of the front, while the converse is true for hydrophones placed south of the front, as well as altering sound propagation path periodicity and focusing.

BIBLIOGRAPHY

1. Cheney, R.E. 1977. Aerial Observations of Oceanic Fronts in the Western Mediterranean Sea, U.S. Naval Oceanographic Technical note 3700-69-77, 30 p.

2. Colborn, J.G. 1975. Mediterranean Sea Acoustic Analysis, unpublished report, Naval Ocean Systems Center, San Diego, California.

3. Director, Naval Oceanography and Meteorology (DNOM). 1976. ASW Oceanographic and Acoustic Support Manual, v. I, Chap. 11.

4. Eubanks, G.E., J.J. Gallagar and D.C. Browning. 1977. The Impact of Ocean Frontal Zones on ASW (A Preliminary Study of Satellite and Ship Observations in the Mediterranean Sea), Naval Underwater Systems Center, New London Laboratory, Technical Memorandum No. 7311(L)-C1-77, 28 p.

5. Fleet Numerical Weather Central. 1977. Oceanographic Services Enviro-Acoustics Products Manual, v. 1, 112 p.

6. Gemmill, W. and E. Khedouri. 1974. A Note on Sound Ray Tracing through a Gulf Stream Eddy in the Sargasso Sea, U.S. Naval Oceanographic Office Technical Note 6150-21-74, 6 p.

7. Khedouri, E. and P. Gaborski. 1977. Acoustic Ray Tracing and Three-Dimensional Propagation Loss Presentation in the Gulf Stream Region, U.S. Naval Oceanographic Office Technical Note 3700-55-76, 21 p.

8. Lanoix, F. 1974. Project Alboran: Hydrological and Dynamic Study of the Alboran Sea, OTAN, No. 66.

9. Levenson, C. and R. Doblar. 1975. An Experiment to Investigate the Effect of the Gulf Stream on Long Range Acoustic Propagation, U.S. Naval Oceanographic Office Technical Note 6150-38-75, 6 p.

10. Lewitt, H.L., J.M. Long and C.A. Hess. 1977. Hydroclimatological Data Retrieval Program, Program Maintenance Manual, Prepared by Ocean Data Systems, Inc. for Fleet Numerical Weather Central.

11. Mommsen, D.B. 1976. Analysis of Sea Surface Temperature Gradients in the Alboran Sea from DMSP and XBT Data, unpublished manuscript from Fleet Weather Central, Rota, Spain, 12 p.

12. Russell, J.J. 1975. A Technique to Summarize Sound Speed Data from the Sea for Application in Acoustic Propagation Loss Models, Naval Undersea Center, San Diego, CA, Technical Note 1553, Chap. 3.

13. Schully-Powers, P., C. Wilson, P. Nysen, P. Andrews, R. Bannister and P. Browning. 1975. Project ANZUS Eddy: Preliminary Report, Royal Australian Navy Research Laboratory.

14. Stephenson, R.E. 1977. Huelva Front and Malaga, Spain Eddy Chain as Defined by Satellite and Oceanographic Data, Sonderdruck aus der Deutschen Hydrographischen Zeitschrift, Band 30, Heft 2, 2 p.

15. Vastano, A.C. and G.E. Owens. 1973. On the Acoustic Characteristics of a Gulf Stream Cyclonic Ring, Journal of Physical Oceanography, v. 3, p. 470-477.

INITIAL DISTRIBUTION LIST

		No. Copies
1.	Defense Documentation Center Cameron Station Alexandria, VA 22314	2
2.	Library, Code 0142 Naval Postgraduate School Monterey, CA 93940	2
3.	Chairman, ASW Group Naval Postgraduate School Monterey, CA 93940	1
4.	Associate Professor R. H. Bourke Department of Oceanography Naval Postgraduate School Monterey, CA 93940	1
5.	LCDR A. B. Chace, USN Department of Oceanography Naval Postgraduate School Monterey, CA 93940	1
6.	LCDR R. P. Adams Patrol Squadron Forty (VP-40) FPO, San Francisco 96601	1
7.	Commander, Fleet Air Mediterranean/ Commander, Task Force Sixty-Seven FPO, New York 09521	1
8.	Commander, Theater Antisubmarine Warfare Forces, Sixth Fleet FPO, New York 09521	1
9.	Commanding Officer (Attn: LCDR D. B. Mommsen) U.S. Fleet Weather Central, Rota, Spain Box 31 FPO, New York 09540	1
10.	Officer in Charge COMASWFORSIXTHFLT Tactical Support Center Rota, Spain Box 37 FPO, New York 09540	1

11. Commanding Officer (Attn: LCDR R. Taranto) 1
Naval Underwater Systems Center
New London Laboratory
New London, Connecticut 06320

12. Office of Naval Research Branch 1
Office, Pasadena (Dr. R. E. Stevenson)
Scientific Liaison Office
University of California, San Diego
La Jolla, CA 92093

13. Director 1
Naval Oceanography and Meteorology
National Space Technology Laboratories
NSTL, Station, MS 39529

14. Commanding Officer 1
Naval Environmental Prediction Research Facility
Monterey, CA 93940

15. Chief of Naval Material 1
ATTN: Manager ASW Systems Project Officer (PM-4)
Navy Department
Washington, DC 20360